

**UNIVERSITÀ CATTOLICA DEL SACRO CUORE
SEDE DI BRESCIA**

Facoltà di Scienze Matematiche, Fisiche e Naturali

Corso di Laurea in Fisica



Tesi di Laurea

**From Dicke to Anderson:
Interplay of Superradiance and Disorder**

Relatore:

Prof. F. Borgonovi

Correlatore:

Dott. G. L. Celardo

Candidato:

Alberto Biella

Matricola n. 3909760

Anno Accademico 2011-2012

Quantum phenomena do not occur in a Hilbert space.

They occur in a laboratory.

— A. Peres

Quantum theory: concepts and methods, 1995

Localization [...], very few believed it at the time,
and even fewer saw its importance,
among those who failed to fully understand it
at first was certainly its author.

It has yet to receive adequate mathematical treatment,
and one has to resort to the indignity of numerical simulations
to settle even the simplest questions about it.

— P.W. Anderson

Nobel Lecture, 1977

Galileo chi si oppose al tuo genio
fu più vil del coyote nel canyon,
se la chiesa ti ha messo all'indice
beh che male c'è tu la metti al medio.

— Caparezza

Il sogno eretico, 2011

Contents

Abstract	v
1 Open quantum systems: superradiance transition	1
1.1 The effective Hamiltonian approach to open quantum systems . . .	2
1.2 Transport proprieties: the scattering matrix	5
1.2.1 How to calculate the transmission matrix	7
1.3 Transition to superradiance	9
2 Disordered system: the Anderson localization	11
2.1 1D Anderson model	12
2.2 An overview on 2D and 3D Anderson model	14
2.2.1 2D Anderson model	14
2.2.2 3D Anderson model	15
3 Interplay of superradiance and disorder in the 1D Anderson model	19
3.1 Introduction	19
3.2 Model	20
3.3 Superradiance transition	23
3.4 Numerical Results	24
3.5 Discussion	28
3.5.1 Perturbative approach for $\kappa \ll 1$	28
3.5.2 Perturbative approach for $\kappa \gg 1$	32
3.6 Further results	36

3.6.1	Structure of the averaged probability distribution in large disorder limit	36
3.6.2	Conductance	43
3.7	Conclusions	45
4	Interplay of superradiance and disorder in the 3D Anderson model	47
4.1	Transition to superradiance	48
4.2	Sensitivity to disorder	49
4.3	Structure of wave functions	55
5	Conclusions	58
	Ringraziamenti	62
	Bibliography	64

Abstract

Nanoscale systems in quantum coherent regime are at the center of many research fields in physics, from quantum computing and cold atoms to transport in nanoscale and mesoscale systems.

The quantum coherence induces the growth of many interesting features. In this thesis we focus our attention on two important consequences of the quantum coherence: Dicke superradiance [1] and Anderson localization [2].

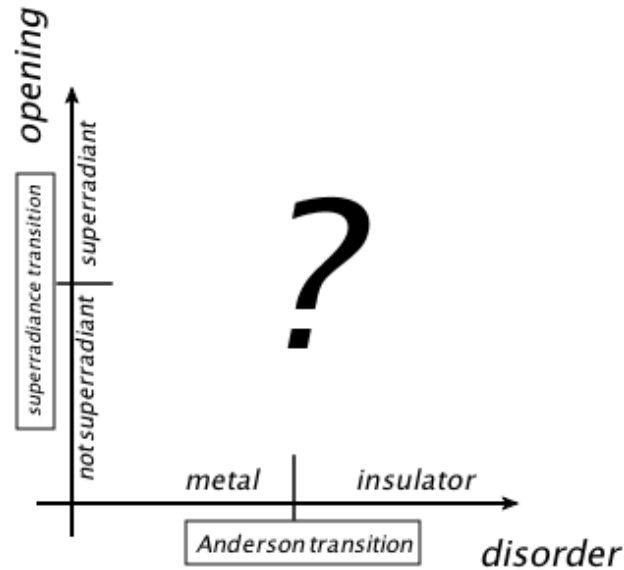


Figure 1: Phases diagram of the problem of the interplay of superradiance and disorder.

Open quantum system can be modeled as a discrete quantum system coupled to an external environment characterized by a continuum of states. As a consequence of the coupling to the continuum the eigenstates acquire a decay width

(finite lifetime). For small coupling all the eigenstates acquire a decay width proportional to the coupling. When a critical value of the coupling is reached the system undergoes a strong change in its resonance structure. Above this critical value of the coupling some eigenstates have non-zero decay width while the decay width of the other eigenstates is approximatively zero.

This phenomena is called transition to superradiance: is due by the opening of the system and induces a segregation of the decay widths of the eigenstates.

On the other hand Anderson transition is driven by intrinsic disorder and induces the exponential localization of the wave functions.

These two phenomena are introduced in Chapter 1 and in Chapter 2 respectively. The effects described in the seminal papers of R. H. Dicke (1954) and P. W. Anderson (1958) have been extensively studied, separately, in the last fifty year. On the other hand the interplay between these two phenomena has not been studied in detail. In other words we know quite well the effects of a variation of the degree of openness of the system (superradiance transition) or the degree of disorder (Anderson transition) separately. What we are going to study is what happens when we vary both the opening and the disorder.

In Figure 1 a picture of the problem of the interplay in terms of phases diagram is shown. If we move along the *opening* axis of the phases diagram, at zero disorder we reach the superradiant regime and then a segregation of the widths occurs, splitting the eigenstates into subradiant and superradiant states. How these two different subspaces are affected by disorder?

Similarly, if we move along the *disorder* axis at zero opening (closed system), we cross the Anderson transition threshold and then all the eigenstates become localized. How these eigenfunctions are sensitive to the opening?

Of course these questions are very general and, even if we are not able to give a fully exhaustive answer, we have addressed here these issues for a particular kind of systems.

In particular, in Chapter 3, we have studied the 1D Anderson model in presence of coherent dissipation, i.e. where a particle hops from site to site in presence of disorder, and escape to any site is allowed. This situation occurs when

the wavelength of the particle is comparable with the sample size and then an effective long-range hopping is created between the sites. In this situation, disorder and opening, have opposite effects: while disorder tends to localize the wave functions, the opening tends to delocalize them, since it induces a long range interaction. In this system we have characterized the structure of the eigenstates in different regimes. The main results is that subradiant and superradiant subspaces are affected by disorder in a very different way.

In Chapter 4 we have studied the same problem in a $3D$ system. In the $3D$ Anderson model the effect of disorder is very different than in $1D$ case since the transition localization-delocalization occurs through a mobility edge. Nevertheless, the features that we have found in the $1D$ system, turn out to be very general and holds in $3D$ model too.

The understanding of this interplay could also play a crucial role in the quest for Anderson localization of light [27] and matter waves [25] even if, due to the generality of our theoretical framework, we believe that it can be useful in the description of all those quantum systems for which the wavelength of the particle is of the same order of the typical length scale of the system.

Chapter 1

Open quantum systems: superradiance transition

In this chapter we present the effective Hamiltonian approach to open quantum systems.

The Effective Hamiltonian, \mathcal{H} , is a powerful tool to take into account the effect of the coupling of a close discrete quantum system to a continuum of states which represent the outside world, for example the continuum of the modes of the electromagnetic field. This method is explained in section 1.1.

Transport proprieties depend on the degree of openness of the system [3, 4, 5, 6] but in important applications the opening is large and can not be treated perturbatively. How the eigenvalues of the effective Hamiltonian affect the transport proprieties is shown in section 1.2 where the scattering matrix, $S(E)$, is analyzed.

The analysis of the complex eigenvalues of \mathcal{H} reveals a general feature of the open quantum systems: the segregation of the decay widths, i.e. the imaginary part of the eigenvalues, after a critical value of the coupling to the continuum. This phenomena is called superradiance transition (ST). The name is due by the analogy with Dicke superradiance in quantum optics [1]. In the section 1.3 this phenomena is explained in detail.

1.1 The effective Hamiltonian approach to open quantum systems

Open quantum system can be modeled as a discrete quantum system coupled to an external environment characterized by a continuum of states.

In order to approach this problem we split the Hilbert space, \mathcal{H} , into two mutually orthogonal subspaces, S_P and S_Q . These subspaces are called *internal subspace* and *external subspace* respectively. The projection operators of a generic state $|\psi\rangle \in \mathcal{H}$ on S_P/Q subspace are P and Q respectively, so we have

$$\begin{aligned} P|\psi\rangle &\in S_P \\ Q|\psi\rangle &\in S_Q. \end{aligned} \quad (1.1)$$

The S_P subspace involves the internal states $\{|n\rangle\}$ labeled by a discrete quantum number $n = 1, \dots, N$. The S_Q subspace involves the external states $\{|c, E\rangle\}$ labeled by a discrete quantum number $c = 1, \dots, M$, which represents the decay channel, and a continuum variable, E , which represents the energy.

Using the projector operators the full Hamiltonian of the system can be written as

$$H_f = PHP + QHQ + PHQ + QHP. \quad (1.2)$$

Using Eq.(1.2) and the fact that $|\psi\rangle = (P + Q)|\psi\rangle$, the stationary Schrödinger equation for the full system read as

$$[PHP + QHQ + PHQ + QHP]|\psi\rangle = E(P + Q)|\psi\rangle. \quad (1.3)$$

Exploiting the proprieties of the projection operators, namely: $PP = P, QQ = Q, PQ = QP = 0$, Eq.(1.3) became

$$(E - PHP)P|\psi\rangle + (E - QHQ)Q|\psi\rangle = QHPP|\psi\rangle + PHQQ|\psi\rangle. \quad (1.4)$$

From multiplication of Eq.(1.4) by P and Q from the left, we obtain respectively

$$(E - PHP)P|\psi\rangle = PHQQ|\psi\rangle \quad (1.5)$$

$$(E - QHQ)Q|\psi\rangle = QHPP|\psi\rangle. \quad (1.6)$$

Our main purpose is to write the Schrödinger equation (1.3) projected into the internal subspace and so we have to eliminate the external states, $Q|\psi\rangle$. In order to do this, from Eq.(1.6) we get

$$Q|\psi\rangle = (E - QHQ)^{-1}QHPP|\psi\rangle \quad (1.7)$$

and we putting it into Eq.(1.5). We obtain

$$\mathcal{H}P|\psi\rangle = EP|\psi\rangle, \quad (1.8)$$

where

$$\mathcal{H} = PHP + PHQ \frac{1}{E - QHQ + i0} QHP, \quad (1.9)$$

is the effective Hamiltonian. To put it in a more clear form we use the explicit form of the projection operators

$$P = \sum_n |n\rangle \langle n|, \quad (1.10)$$

$$Q = \sum_c \int dE' |c, E'\rangle \langle c, E'| \quad (1.11)$$

and multiply from the left by the external state $\langle m|$. What we get is

$$\langle m|\mathcal{H}(E)|n\rangle = \langle m|H|n\rangle + \sum_c \int dE' \frac{A_m^c(E')A_n^c(E')^*}{E - E' + i0}, \quad (1.12)$$

where $A_n^c(E) \equiv \langle n|PHQ|c, E\rangle$ represents the coupling amplitudes between the internal and the external states.

The integral in Eq.(1.12) can be decomposed, using the Sokhotski-Plemelj formula¹, into its Hermitian part (principal value) and the remaining non-Hermitian part, using

$$\sum_c \int dE' \frac{A_m^c(E')A_n^c(E')^*}{E - E' + i0} = \sum_c \mathcal{P} \int dE' \frac{A_m^c(E')A_n^c(E')^*}{E - E'} - i\pi \sum_{c \text{ (open)}} A_m^c(E)A_n^c(E)^*. \quad (1.14)$$

¹Let f be a complex-valued function, let a and b real and $a < 0 < b$. Then

$$\lim_{\varepsilon \rightarrow 0^+} \int dx \frac{f(x)}{x \pm i\varepsilon} = \mathcal{P} \int dx \frac{f(x)}{x} \mp i\pi f(0), \quad (1.13)$$

where \mathcal{P} stand for the Cauchy principal value.

Now we are able to write the effective non-Hermitian Hamiltonian as follow

$$\mathcal{H}(E) = H_0 + \Delta(E) - \frac{i}{2}W(E), \quad (1.15)$$

where

$$(H_0)_{mn} = \langle m|H|n\rangle, \quad (1.16)$$

$$\Delta_{mn} = \sum_c \mathcal{P} \int dE' \frac{A_m^c(E')A_n^c(E')^*}{E - E'}, \quad (1.17)$$

$$W_{mn} = 2\pi \sum_{c \text{ (open)}} A_m^c(E)A_n^c(E)^*. \quad (1.18)$$

If we restrict our analysis into a small energy windows we can do some useful simplification. In fact if we assume that $\Delta(E)$ and $W(E)$ are smooth function of E we can neglect their energy dependence. Therefore the coupling amplitudes, A_n^c , becomes energy independent parameters. For simplicity, in this work, we have neglected the energy shift term, Δ .

In conclusion, the effective Hamiltonian that we use in order to study the coupling of a discrete quantum system to a environment is:

$$\mathcal{H} = H_0 - \frac{i}{2}W, \quad W_{mn} = 2\pi \sum_{c=1}^M A_m^c A_n^{c*}. \quad (1.19)$$

The interpretation of Eq.(1.19) is the follow: the Hermitian part, H_0 , represent the *close* discrete quantum system. The non-Hermitian part, W , describes the coupling to the continuum of N intrinsic states through M open decay channels.

The eigenvalues of \mathcal{H} are complex

$$\mathcal{E}_r = E_r - \frac{i}{2}\Gamma_r, \quad (1.20)$$

where Γ_r is the decay width of the state. In this approach, the decay width Γ_r , has to be interpreted as the inverse of a characteristic lifetime ($\Gamma_r/\hbar = 1/\tau_r$) of an eigenstate $|r\rangle$. Indeed it can be proved that the time evolution of $|r\rangle$ is driven by \mathcal{H} , so that

$$|r(t)\rangle = e^{-\frac{i}{\hbar}\mathcal{H}t}|r\rangle$$

$$= e^{\frac{i}{\hbar}E_r t} e^{-\frac{\Gamma_r}{2\hbar}t} |r\rangle. \quad (1.21)$$

Equation (1.21) clearly show that if at $t = 0$ the particle is in the state $|r\rangle$ after a time t the probability of find the particle still in this state is

$$P_r(t) = e^{-\frac{\Gamma_r}{\hbar}t}. \quad (1.22)$$

1.2 Transport proprieties: the scattering matrix

The aim of this section is to show why the transport propriety of the system are strongly affected by the eigenvalues \mathcal{E}_r of \mathcal{H} . In order to do this we analyze the structure of the scattering matrix, $S(E)$. The scattering matrix can be deduced in a straightforward manner from \mathcal{H} . First of all consider Eq.(1.2) and rewrite the full Hamiltonian, H_f , as follows

$$H_f \equiv H_w + V, \quad (1.23)$$

where $H_w \equiv PHP + QHQ$ is the part of the full Hamiltonian acting within the relative subspace while, $V \equiv PHQ + QHP$, acts across internal and external subspaces. From standard scattering theory we know that the scattering matrix is defined as

$$S(E) = 1 - \mathcal{T}(E), \quad (1.24)$$

where \mathcal{T} is the transmission matrix. From Eq.(1.23) and using the Lippmann-Schwinger equation we can write the transmission matrix as

$$\mathcal{T}(E) = V + V \frac{1}{E - H_f + i0} V. \quad (1.25)$$

In accord with Eq.(1.25) the transition amplitude for the process $b \rightarrow a$ is given by

$$\mathcal{T}^{ab}(E) = \langle a, E' | \mathcal{T} | b, E' \rangle \quad (1.26)$$

$$= \langle a, E' | V | b, E' \rangle + \langle a, E' | V \frac{1}{E - H_f + i0} V | b, E' \rangle. \quad (1.27)$$

Now, using the orthogonality between the two subspaces and the properties of the projection operators we find

$$\mathcal{T}^{ab}(E) = \langle a, E' | QHPP \frac{1}{E - H_f + i0} PPHQ | b, E' \rangle. \quad (1.28)$$

The operator $P(E - H_f + i0)^{-1}P$ is the projection in the internal subspace of the full Hamiltonian propagator. This projection of the full Hamiltonian in the internal subspace is exactly what we have done in the Sec.1.1 and leads to effective Hamiltonian. Of course the projection $H_f \rightarrow \mathcal{H}$ readily leads to the projection of the propagators,

$$H_f \rightarrow \mathcal{H} \implies \frac{1}{E - H_f} \rightarrow \frac{1}{E - \mathcal{H}}. \quad (1.29)$$

After this operation the transmission matrix can be written as

$$\begin{aligned} \mathcal{T}^{ab}(E) &= \langle a, E' | QHP \frac{1}{E - \mathcal{H}} PHQ | b, E' \rangle \\ &= \sum_{n,m=1}^N \langle a, E' | QHP | n \rangle \langle n | \frac{1}{E - \mathcal{H}} | m \rangle \langle m | PHQ | b, E' \rangle \\ &= \sum_{n,m=1}^N A_n^{a*} \left(\frac{1}{E - \mathcal{H}(E)} \right)_{nm} A_m^b. \end{aligned} \quad (1.30)$$

From the matrix of the transmission amplitude, \mathcal{T}^{ab} , we can define the *transmission* from channel b to channel a :

$$\mathsf{T}^{ab} = |\mathcal{T}^{ab}|^2. \quad (1.31)$$

In order to show that the eigenvalues of \mathcal{H} coincide with the poles of scattering matrix, $S = 1 - i\mathcal{T}$, we have to rewrite Eq.(1.30) on the basis of the eigenstates of \mathcal{H} . We start with its diagonalization. Eigenstates of \mathcal{H} form a bi-orthogonal complete set such as

$$\mathcal{H} |r\rangle = \mathcal{E}_r |r\rangle, \quad \langle \tilde{r} | \mathcal{E}_r^* = \langle \tilde{r} | \mathcal{H}, \quad (1.32)$$

with $\langle \tilde{r} | \neq |r\rangle^*$ and where the eigenvalues are complex

$$\mathcal{E}_r = E_r - \frac{i}{2}\Gamma_r. \quad (1.33)$$

Hence on the basis of its eigenstates the propagator transforms as

$$(E - \mathcal{H})_{nm}^{-1} \rightarrow (E - \mathcal{E}_r)^{-1} \delta_{r,r'}. \quad (1.34)$$

The coupling amplitudes transform similary

$$A_m^b \rightarrow \mathcal{A}_r^b = \sum_{m=1}^N A_m^b \langle m|r \rangle, \quad A_n^{a*} \rightarrow \tilde{\mathcal{A}}_r^b = \sum_{n=1}^N A_n^{a*} \langle \tilde{r}|n \rangle. \quad (1.35)$$

Armed with Eq.(1.34) and Eq.(1.35) the expression for the \mathcal{T} matrix becomes

$$\mathcal{T}^{ab}(E) = \sum_{r=1}^N \frac{\tilde{\mathcal{A}}_r^a \mathcal{A}_r^b}{E - \mathcal{E}_r}. \quad (1.36)$$

It's easy to see, from Eq.(1.36), that the poles of the S matrix coincide with the eigenvalues of \mathcal{H} . This observation show us that the position in the complex plane of \mathcal{E}_r strongly affects the transport propieties of the system.

1.2.1 How to calculate the transmission matrix

In order to calculate the conductance of the system we need to know the transmission matrix \mathcal{T} . In the previous chapter we have shown that \mathcal{T} is a $M \times M$ matrix, where M is the number of open channels, of the form,

$$\mathcal{T}^{ab}(E) = \sum_{m,n=1}^N A_n^{a*} \left(\frac{1}{E - \mathcal{H}} \right)_{nm} A_m^b, \quad (1.37)$$

The method to calculate the \mathcal{T} matrix naturally implies the diagonalisation of the effective Hamiltonian for any disordered realization and for each energy too if we consider the energy dependent formalism. In this section we will show a new method, developed by S. Sorathia [9], that involved only the diagonalisation of the Hermitian part, H , of effective Hamiltonian for any configuration. This is important because the numerical diagonalisation of an Hermitian matrix is much faster than for a non-Hermitian one.

The effective Hamiltonian can be written as,

$$\mathcal{H} = H - \frac{i}{2}W. \quad (1.38)$$

where the anti-Hermitian part has the factorised form $W = 2\pi AA^T$. The matrix A is a rectangular $N \times M$ matrix with columns composed of $A_n^c(E)$. Now we introduce the resolvents, for the closed and for the open system, respectively,

$$G = \frac{1}{E - H}, \quad \mathcal{G} = \frac{1}{E - \mathcal{H}}. \quad (1.39)$$

Since $\mathcal{H} = H - i\pi A^T A$ the relation between G and \mathcal{G} becomes

$$\mathcal{G} = G - i\pi G A \frac{1}{1 + i\pi K} A^T G, \quad (1.40)$$

where we have defined the $M \times M$ matrix $K = A^T G A$. Eq. (1.40) can be easily deduced using the Woodbury matrix identity,

$$(B + UCV)^{-1} = B^{-1} - B^{-1}U(C^{-1} + VB^{-1}U)^{-1}VB^{-1}. \quad (1.41)$$

Now we can substitute the relation (1.40) in the definition of transmission matrix (1.37),

$$\begin{aligned} \mathcal{T} &= A^T \mathcal{G} A \\ &= A^T G A - i\pi A^T G A \frac{1}{1 + i\pi K} A^T G A \\ &= K - i\pi K \frac{1}{1 + i\pi K} K \\ &= \frac{K}{1 + i\pi K}. \end{aligned} \quad (1.42)$$

In order to evaluate $K = A^T G A$, and then \mathcal{T} , one have to diagonalise the Hermitian Hamiltonian H and to write the matrix A in the basis of H . Using the transformation matrix V , which has as columns the eigenstates of H , we can write A in the new basis

$$\tilde{A} = V^T A \implies \tilde{A}_n^c = \sum_m A_m^c \phi_m(E_n), \quad (1.43)$$

where $\phi_m(E_n)$ stands for the m^{th} component of the n^{th} eigenvector of H with eigenvalue E_n . This change of basis allow us to write the K -matrix as

$$K^{ab} = \left(\tilde{A}^T \frac{1}{E - H} \tilde{A} \right)^{ab}$$

$$= \sum_{n=1}^N \frac{\tilde{A}_n^a \tilde{A}_n^b}{E - E_n}. \quad (1.44)$$

The \mathcal{T} matrix can be obtained in a straightforward way from Eq.(1.42).

In conclusion we can state that the method explained above allow the explicit calculation of \mathcal{T} matrix by the diagonalisation of one internal Hermitian Hamiltonian only. This is a powerful tool from the numerical point of view and we are reduced to invert the $M \times M$ matrix $1 + i\pi K$ for each value of E only. In our models M is small and this the inversion is very fast.

1.3 Transition to superradiance

Let us start from a simplified version of Eq.(1.19),

$$\mathcal{H} = H_0 - i\frac{\gamma}{2}W, \quad (1.45)$$

where

$$W_{ij} = \sum_{c=1}^M A_i^c A_j^{c*}, \quad (1.46)$$

γ is the parameter controlling the coupling to continuum of states of external world and the basis $\{|i\rangle\}$ are the eigenstates of H_0 with eigenvalues E_i^0 (and thus H_0 is diagonal in this representation with $(H_0)_{ii} = E_i^0$). We can treat W as a perturbation if $\gamma/D \ll 1$ where D is the mean level spacing between neighboring eigenstates of H_0 . This condition is always true if $\langle\Gamma\rangle/D \ll 1^2$. Under this condition the eigenvalues of \mathcal{H} at the first order in perturbation theory are

$$\mathcal{E}_i = E_i^0 - i\frac{\gamma}{2}W_{ii}. \quad (1.48)$$

Eq.(1.48) state that when $\langle\Gamma\rangle/D \ll 1$ *all* the state acquire a decay width proportional to γ . In the limit $\gamma \gg 1$ we have that W is the leading term and H_0 can be

² Where $\langle\Gamma\rangle$ is the *average width* defined as

$$\langle\Gamma\rangle = \frac{1}{N} \sum_{r=1}^N \Gamma_r. \quad (1.47)$$

. Of course $\langle\Gamma\rangle$ depends of γ . For example if $W_{ij} = 1 \ \forall i, j$ we have $\langle\Gamma\rangle = \gamma$.

viewed as a perturbation. The structure of W (see Eq(1.46)) allow one to deduce that the rank of W and thus also of \mathcal{H} is M , the number of open channels. From this simple consideration we can state that W has only M non-zero eigenvalues if $M < N$. Thus in the limit of large coupling to continuum only M out of N states will have a non-zero decay width. These state are called *short-lived* states (*superradiant* states). The decay width of the others $N - M$ states approach zero in this regime, and thus are decoupled from the continuum of states, for this reason they are called *long-lived* states (or *subradiant* states).

Summarizing: for small coupling to continuum, $\langle \Gamma \rangle / D \ll 1$, all states acquire a decay width proportional to γ (as predicted by first order perturbation theory). When the coupling to the continuum reaches a critical value, only M eigenvalues continue to increase their width while the others $N - M$ eigenvalues start to decrease their width. Finally, in the limit of large coupling, $\langle \Gamma \rangle / D \gg 1$, only M states have a non-zero decay width and the decay width of the others $N - M$ states are approximately zero. We could say that the system in order to survive to the opening has to rearrange itself. The opening then induce a segregation of the imaginary part of the eigenvalues of \mathcal{H} . This phenomenon is called *superradiance transition* (ST)³. The transition to superradiance is expected to occur for

$$\frac{\langle \Gamma \rangle}{D} \approx 1. \quad (1.49)$$

The criterium (1.49) for the transition to superradiance is valid in the case of uniform energy and negligible energy shift.

³ The name is due by the analogy with Dicke superradiance in quantum optics.

Chapter 2

Disordered system: the Anderson localization

Ordered structures have been studied since the beginning of Quantum Mechanics. This is because the periodicity of such materials, and then of the interactions, allow one to employ the Bloch theorem (see Ref.[24]). In this way the structure of the eigenstates of rather complicated crystalline materials can be calculated. In the real world perfect crystals are an exception: disorder, in different degrees, is almost always present. In solid state physic the disorder can be caused, for example, by few impurities in an otherwise perfect crystalline host (weak disorder). In the opposite limit, if we think about alloys or glassy structure, we have an example of strongly disordered materials.

In this chapter we briefly explain the concept of intrinsic disorder in a quantum system and then of the Anderson localization. The microscopic theory of Anderson localization [2] is far from trivial and after fifty years is not fully understood. However for our purpose is sufficient to understand the consequence of the introduction of the disorder on the structure of the wave functions.

2.1 1D Anderson model

We start from a paradigmatic example that show how the disorder can change drastically the structure of the eigenstates of a system. Consider a one-dimensional Anderson model [2, 10] with diagonal disorder in the tight binding approximation, for the motion of a particle in a disordered potential. The Anderson Hamiltonian can be written as

$$H_0 = \sum_{j=1}^N E_j |j\rangle \langle j| + \Omega \sum_{j=1}^{N-1} (|j\rangle \langle j+1| + |j+1\rangle \langle j|), \quad (2.1)$$

where E_j are random variables uniformly distributed in $[-W/2; W/2]$ and Ω is the tunnel transition amplitude to nearest neighbors sites. This mean that each site, $|j\rangle$, has a random energy E_j but the tunnel transition amplitude to nearest neighbor sites, Ω , remains constant. Of course, the disorder strength is W , and if $W = 0$ the system is ordered. In the case of a ordered chain, $W = 0$, the eigenstates are extended waves

$$\psi_q(j) = \sqrt{\frac{2}{N+1}} \sin\left(\frac{\pi q}{N+1} j\right), \quad (2.2)$$

and the relative eigenvalues are

$$E_q = -2\Omega \cos\left(\frac{\pi q}{N+1}\right), \quad (2.3)$$

where $q = 1, \dots, N$ is a quantum number and $j = 1, \dots, N$ is a discrete coordinate.

If $W \neq 0$ the structure of the eigenstates change drastically: a 1D infinite tight-binding chain with a random diagonal potential will cause *all* eigenstates of the system to get localized exponentially, even for weak amplitude of fluctuations. This means that the envelope of the eigenstate $\psi_q(j)$ is centered on some site j_0 with the tails that approximatively decay exponentially:

$$|\psi_q(j)| \sim \exp\left(-\frac{|j-j_0|}{\xi}\right), \quad (2.4)$$

where ξ is the *localization length* of the eigenstate and is a measure of a typical spatial extension of the eigenstate.

This fact can be intuitively understood using the perturbation theory at first order: a zeroth-order description of the eigenstate would be a bound state or a

localized orbital bound by deep fluctuation in the random potential. We could then consider the admixture between different orbitals, Ω , as a perturbation. The main point is that such admixture will not produce an extended state composed of linear combinations of infinitely many localized orbitals, as in the case $W = 0$. The reason is that orbitals that are close in space, so that the wave functions overlap significantly (in the tight binding approximation only the nearest neighbors), are in general very different in energy, so that the admixture is small because of the large energy denominator¹. On the other hand, states that are nearly degenerate are in general very far apart in space, so that the overlap is very small [10].

However if the localization length is greater than the system size ($\xi > N$) we say that the state is extended. For this reason also in one-dimensional case we can define a size-dependent critical strength of disorder, W_c , such that $\xi = N$ in a certain position of the band.

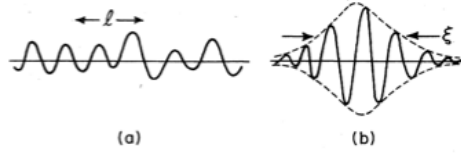


Figure 2.1: (a) Typical extended wave function with mean free path l ; (b) localized state with localization length ξ .

In the case of 1D Anderson model with weak uncorrelated diagonal disorder it is possible to find a closed expression for ξ . Thouless was the first to do it in the case of an infinite chain. He found an expression for ξ in terms of the variance, σ^2 , of the site energies distribution [7]:

$$\xi = \frac{8(1 - (E/2\Omega)^2)}{\sigma^2} \Omega^2. \quad (2.5)$$

¹ At the first order in perturbation theory an eigenstate of the full Hamiltonian (unperturbed Hamiltonian plus a perturbation) is given by the eigenstate of the unperturbed Hamiltonian plus a superposition of all other unperturbed eigenstates that overlap significantly with it, weighted over their energy difference.

In the case of uniform distribution centered around zero we have

$$\sigma^2 = \langle E_j^2 \rangle = \frac{W^2}{12}, \quad (2.6)$$

and then the localization length reads as

$$\xi = 96(1 - (E/2\Omega)^2) \left(\frac{\Omega}{W} \right)^2. \quad (2.7)$$

For $E = 0$, Eq.(2.7) has to be modified and we have [13]

$$\xi(E = 0) = 105.2 \dots \left(\frac{\Omega}{W} \right)^2. \quad (2.8)$$

Our numerical simulations are in agreement with Eq.(2.7) in the limit of weak disorder ($\sigma^2 \ll 1$) and far from the band edges ($|E| \ll 2\Omega$).

2.2 An overview on 2D and 3D Anderson model

The number of spatial dimensions strongly affects the phenomenon of localization. In this section we give an overview of the main results about the 2D and 3D Anderson model. In both cases the Hamiltonian is similar to (2.1), i.e. a tight binding model with diagonal uncorrelated disorder. Of course the interaction Ω should be extended to nearest neighbors that are 4 (6) in 2D (3D) case.

2.2.1 2D Anderson model

In a two-dimensional Anderson model we have that for any $W > 0$ *all* the eigenstates are exponentially localized like in 1D case.

In Figure 2.2 is shown the behavior of ξ as a function of position in the energy band for fixed strength of disorder. There is no an explicit expression for ξ as a function of all parameters (W and E). Nevertheless in the center of the energy band and for weak disorder, the localization length behaves as

$$\ln \xi(E = 0) \propto \frac{1}{W^2}. \quad (2.9)$$

For the detail of derivation of Eq.(2.9) see [22]. In Figure 2.3 (taken from [22]), we show $\log \xi$ vs. W^{-2} . As you can see Eq.(2.9) is verified for small W (large W^{-2}) values.

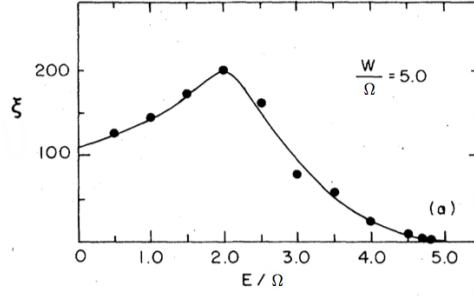


Figure 2.2: Localization length ξ versus energy E/Ω for a square lattice. Full circles are the numerical results while the thick solid line is the theoretical prediction (taken from Ref. [20]).

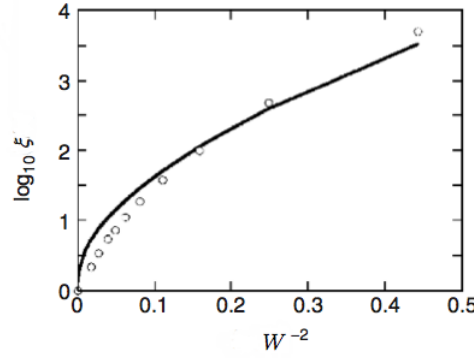


Figure 2.3: Localization length ξ as a function of $1/W^2$ for the 2D Anderson model. Here is $E = 0$. Open circles are the numerical results while the solid line is the theoretical prediction.

2.2.2 3D Anderson model

The effect of disorder in the 3D model is very different from the 1D and 2D cases. For very large disorder all (or almost all) states are localized but for small disorder the situation is different: the states in the middle of the energy band are extended while the states close to the band edges may be localized, see Figure 2.4 [21]. The thresholds E_{m1} and E_{m2} are called *mobility edges*.

The position in the energy band of E_{m1} and E_{m2} depends on the ratio W/Ω . On increasing W/Ω , the mobility edges approach one to each other and coalesce at

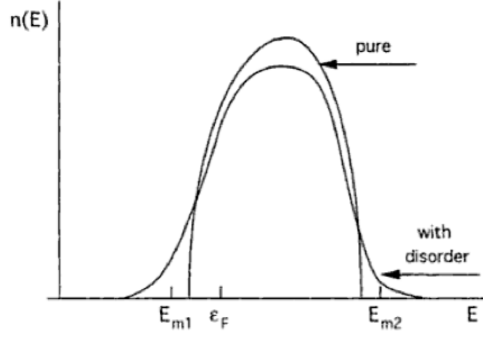


Figure 2.4: Density of states $n(E)$ for $W = 0$ (pure) and $W \neq 0$ (with disorder) and the mobility edges in the former case.

some critical value W_c , where all states became localized and Anderson transition occurs. This result was shown numerically for the first time by A. D. Zdetsis *et al.* [20], see Figure 2.5. It is also possible to find that for the 3D Anderson model

$$\frac{W_c}{\Omega} \approx 16.5. \quad (2.10)$$

For finite size sample (N) we define the *localized regime* when $\xi/N < 1$.

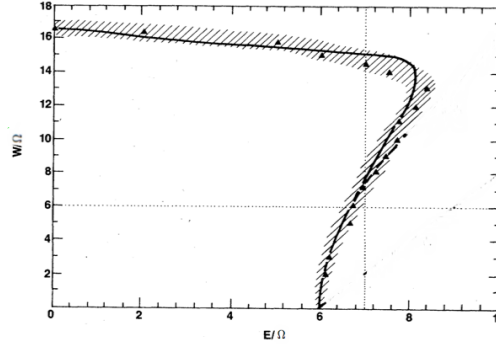


Figure 2.5: Dependence of the mobility edge of diagonal disordered W for a cubic lattice. Solid triangles are the numerical results while the thick solid line is the theoretical prediction. The dotted straight lines indicate the independent variables for Fig. 2.6

Close to the critical point, i.e. when $W - W_c \ll 1$ and $W > W_c$, the behavior of

ξ is given by

$$\xi \propto \frac{1}{W - W_c}. \quad (2.11)$$

For the details about the theoretical derivation of Eq.(2.11) see [22] and the references therein.

The localization length, ξ , also depends on both the eigenvalues position in the energy band and W . Even in this case a closed analytical expression of ξ as a function of both E and W is not know. However in [20] the results of numerical simulation was fitted in order to provide an expression for the localization length:

$$\xi \approx \frac{A\phi + B}{1 - \phi} l, \quad (2.12)$$

where

$$A = 14.2$$

$$B = 2.20$$

$$\phi = Sl^2/8.96 \quad (2.13)$$

where S is the constant energy surface and l is the mean free path ². Using the coherent potential approximation (CPA) to calculate S and l for a given pair of E and W and then substituting into Eq.(2.12) an explicit expression for ξ is obtained. The localization length, ξ , as a function of W and E is shown in Figure 2.6.

² Here both S and l have to be expressed in units of lattice constant and then are adimensional quantities.

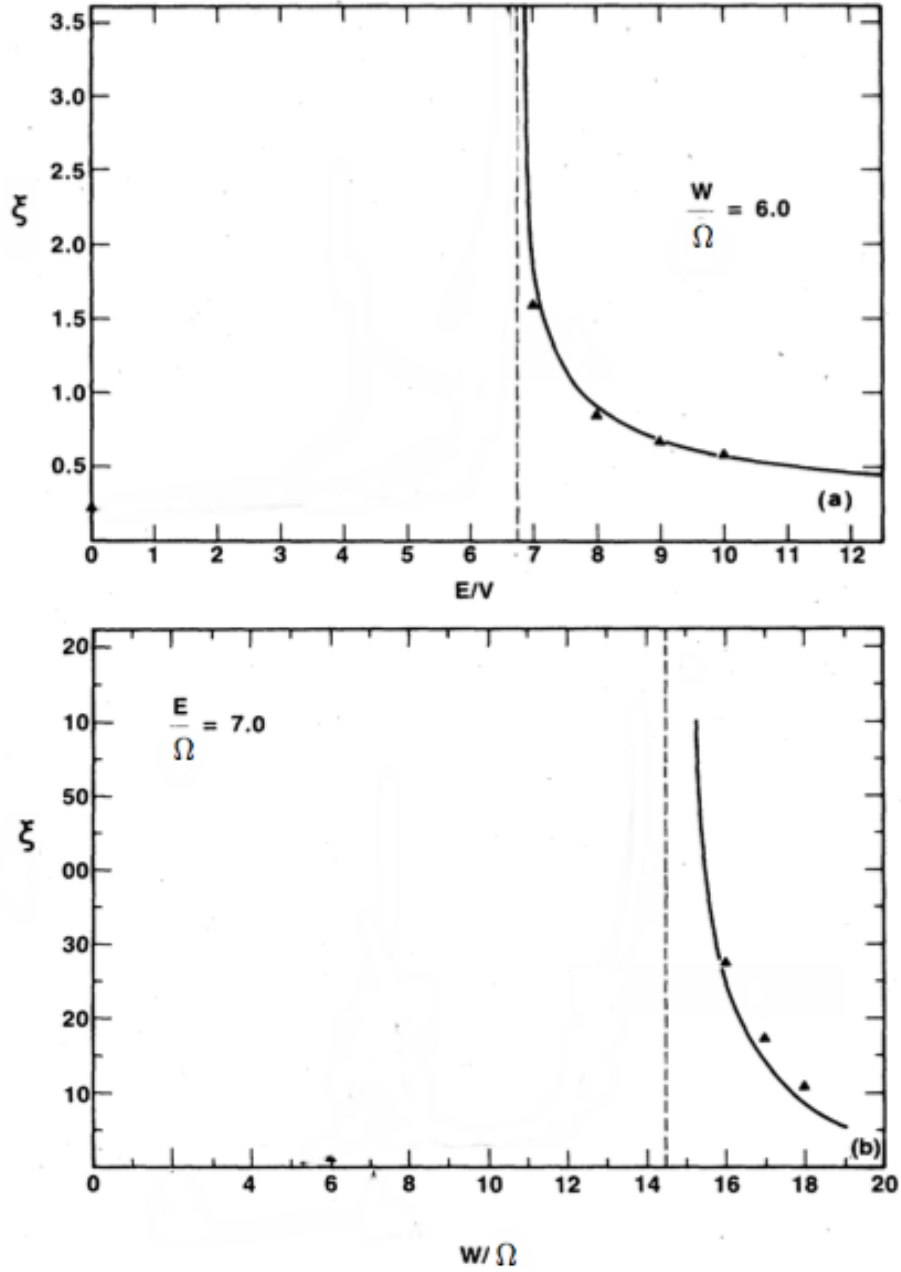


Figure 2.6: (a) Localization length ξ as a function of energy E/Ω for a cubic lattice with disorder $W/\Omega = 6.0$. (b) Localization length ξ versus the strength of diagonal disorder W/Ω for a cubic lattice for energy $E/\Omega = 7.0$. In both cases solid triangle are the numerical results while thick solid line is the theoretical prediction.

Chapter 3

Interplay of superradiance and disorder in the 1D Anderson model

Using a non-Hermitian Hamiltonian approach to describe open systems, we study the interplay of disorder and superradiance in a one-dimensional Anderson model. Analyzing the complex eigenvalues of the non-Hermitian Hamiltonian, a transition to a superradiant regime is shown to occur. As an effect of openness the structure of eigenstates undergoes a strong change in the superradiant regime: we show that the sensitivity to disorder of the superradiant and the subradiant subspaces is very different; superradiant states remain delocalized as disorder increases, while subradiant states are sensitive to the degree of disorder.

3.1 Introduction

In this work we analyze a one-dimensional Anderson model, where a particle hops from site to site in presence of disorder, and is also allowed to escape the system from any site. When the wavelength of the particle is comparable with the sample size, an effective long-range hopping is created between the sites. This coupling can induce the ST, which affects in a non-trivial way the transport properties of the system. Similar models of quantum transport with coherent dissipation have been already considered in the literature [16], but a detailed analysis of the interplay

of localization and superradiance is still lacking. Preliminary investigations have been recently done in Ref. [15, 3, 5], but there the particle was allowed to escape only from the end sites, while in the situation analyzed in this work, all sites are coupled to the external environment. This situation occurs in many important physical situations, such as in cold atoms, where a single photon is injected in the atomic cloud [11], or in quantum dots [17].

Intrinsic disorder and opening to the environment have opposing effects: while disorder tends to localize the wave functions, the opening tends to delocalize them, since it induces a long range interaction. The aim of this paper is to study the interplay of disorder and opening, and the relation to superradiance. We show that while below the ST, all states are affected by disorder and opening in a similar way, above it, the effects are quite different for superradiant and subradiant subspaces, the latter being more affected by disorder than the former.

In Sec. 3.2 we introduce the model, in Sec. 3.3 we analyze the ST in our system, and in Sec. 3.4 we present our main numerical results, which we partly justify in Sec. 3.5 using perturbation theory. Finally in Sec. 3.7 we present our conclusions.

3.2 Model

Our starting point is the standard one-dimensional Anderson model [2, 10], for the motion of a particle in a disordered potential. The Hamiltonian of the Anderson model can be written as:

$$H_0 = \sum_{j=1}^N E_j |j\rangle\langle j| + \Omega \sum_{j=1}^{N-1} (|j\rangle\langle j+1| + |j+1\rangle\langle j|), \quad (3.1)$$

where E_j are random variables uniformly distributed in $[-W/2, +W/2]$, W is a disorder parameter, and Ω is the tunneling transition amplitude (in our numerical simulations we set $\Omega = 1$). As we have already shown in chapter 2 for $W = 0$ the eigenstates are extended and we have for the eigenvalues:

$$E_q = -2\Omega \cos\left(\frac{\pi q}{N+1}\right), \quad (3.2)$$

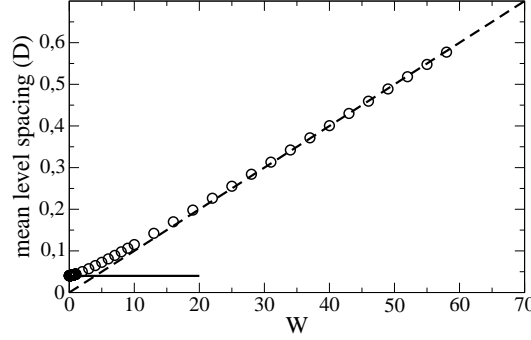


Figure 3.1: The mean level spacing D versus W . The solid line is $4\Omega/N$ while the dashed line is W/N . Each point is obtained averaging over 10^3 realizations. Here $\Omega = 1$, $N = 100$ and $\gamma = 0$.

and the eigenstates:

$$\psi_q(j) = \sqrt{\frac{2}{N+1}} \sin\left(\frac{\pi q}{N+1} j\right), \quad (3.3)$$

where $q = 1, \dots, N$ is a quantum number and $j = 1, \dots, N$ is a discrete coordinate. In this case, the eigenvalues lie in the interval $[-2\Omega, 2\Omega]$, so the mean level spacing can be estimated as $D = 4\Omega/N$. The mean level spacing D as a function of W for the closed model is shown in Figure 3.1. For $W \neq 0$, the eigenstates of the one-dimensional Anderson model are exponentially localized on the system sites, with exponential tails given by $|\psi(j)| \sim \exp(-|j - j_0|/\xi)$, and for weak disorder, the localization length ξ can be written as:

$$\xi \approx 96 (1 - (E/2\Omega)^2) \left(\frac{\Omega}{W}\right)^2. \quad (3.4)$$

For $E = 0$, Eq. (3.4) has to be modified and we have:

$$\xi \approx 105.2 \left(\frac{\Omega}{W}\right)^2.$$

The phenomenon of Anderson localization was studied in a closed disordered chain, while in our case we can vary the degree of openness of the system. In par-

ticular we consider the model in which all sites are coupled to a common channel in the continuum, with equal coupling strength γ . This situation can arise when the wavelength of the decaying particle is much larger than the size of the system. This results in a coherent dissipation, which differs from the usual dissipation where every site decays independently to a different channel in the continuum. A comparison between these two different mechanisms will be the subject of a future work. As we have explained in Chapter 1 the continuum coupling can be taken into account with the aid of an effective non-Hermitian Hamiltonian, which in general can be written as,

$$\mathcal{H}(E) = H_0 + \Delta(E) - iQ(E),$$

where H_0 is the Hermitian Hamiltonian of the closed system decoupled from the environment and $\Delta(E)$ and $Q(E)$ are the induced energy shift and the dissipation, respectively. Neglecting the energy dependence and the energy shift we have

$$\mathcal{H}_{ij} = (H_0)_{ij} - \frac{i}{2} \sum_c A_i^c (A_j^c)^*, \quad (3.5)$$

where A_i^c are the transition amplitudes from the discrete states i to the continuum channels c .

In the case under study, we have only one decay channel, $c = 1$, and all couplings are equal, so that $A_i^1 = \sqrt{\gamma}$. Thus the effective Hamiltonian can be written as:

$$\mathcal{H} = H_0 - i\frac{\gamma}{2}Q, \quad (3.6)$$

where H_0 is the Anderson Hamiltonian with diagonal disorder, Eq. (3.1), and $Q_{ij} = 1 \forall i, j$.

In order to study the interplay of Anderson localization and superradiance we analyze the participation ratio (PR) of the eigenstates of \mathcal{H} , defined as,

$$PR = \left\langle \frac{1}{\sum_i |\langle i | \psi \rangle|^4} \right\rangle, \quad (3.7)$$

where the average is over disorder.

The PR is a measure of the degree of the spatial extension of wave function. For example if we consider the completely delocalized state $|\psi\rangle = \frac{1}{\sqrt{N}}(1, \dots, 1)^T$

we have $PR = N$. In the opposite limit, for a state localized only on a certain site we have $PR = 1$. All the other kinds of states should have $1 \leq PR \leq N$. For example, the eigenstates of H_0 (closed system) for $W = 0$ are the so called Bloch waves, see Eq.(3.3). These eigenstates are extended but not completely delocalized. If we compute the PR in large N limit we obtain $PR = 2N/3$ for any eigenstates [13]. Is important to note that in principle the PR does not provide us any information about the structure of a state. Also the phase correlation between the component of a state is completely neglected by the PR .

3.3 Superradiance transition

ST can be analyzed by studying the complex eigenvalues $\mathcal{E}_r = E_r - i\Gamma_r/2$ of \mathcal{H} defined in Eq. (3.6). As the coupling between the states and the continuum increases, one observes a rearrangement of the widths Γ_r . ST is expected to occur for $\langle \Gamma \rangle / D \simeq 1$. The average width, $\langle \Gamma \rangle$, is given by γ , so we can define

$$\kappa = \gamma/D \quad (3.8)$$

as the effective parameter controlling the coupling strength to the continuum. In the deep localized regime where disorder is strong ($W \gg \Omega$) we can write $D \approx W/N$, so that the effective coupling strength can be written as:

$$\kappa = \frac{\gamma N}{W} \quad (3.9)$$

In Fig. 3.2 we show that ST occurs at $\kappa \sim 1$ for different values of W/Ω and N .

For $\kappa \gg 1$, we can treat the matrix Q as the leading term in Eq. (3.6), and H_0 as a perturbation. The superradiant state $|SR\rangle$ is given to zeroth order by the eigenstate of Q with nonzero eigenvalue: $|d\rangle = \frac{1}{\sqrt{N}}(1, \dots, 1)^T$, and the energy of $|SR\rangle$ is evaluated at the first order as

$$\langle d | \mathcal{H} | d \rangle = \varepsilon - i\frac{\gamma}{2}N, \quad (3.10)$$

where

$$\varepsilon = \frac{1}{N} \sum_{i=1}^N E_i + 2\Omega \frac{N-1}{N}$$

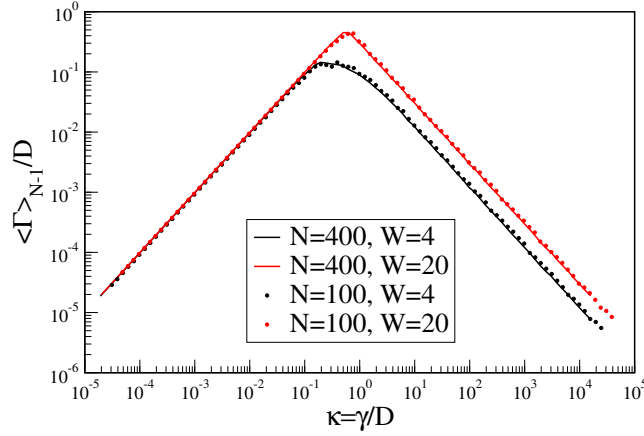


Figure 3.2: The average width of the $N - 1$ subradiant states, normalized by the mean level spacing D , versus the effective coupling strength κ for different values of N and W , and $\Omega = 1$. Here we average over 100 disordered configurations.

and E_i are the random diagonal elements of H_0 . Averaging over disorder and taking into account that E_i are distributed uniformly in $[-W/2, W/2]$ we obtain,

$$\langle \epsilon \rangle = 2\Omega \frac{N-1}{N} \quad (3.11)$$

and

$$\text{Var}(\epsilon) = \langle \epsilon^2 \rangle - \langle \epsilon \rangle^2 = \frac{W^2}{12N}. \quad (3.12)$$

These results agree with our numerical simulations for different values of N and allow one to know the position in the energy band of the superradiant state in the limit $\kappa \gg 1$. From Eq. (3.11) we deduce that the mean energy $\langle \epsilon \rangle$ of the superradiant state is independent of W .

3.4 Numerical Results

In order to study the interplay of superradiance and disorder we have analyzed the *PR* of the eigenstates of the non-Hermitian Hamiltonian, Eq. (3.6).

As explained in the previous section, as the coupling with the continuum is increased we have the formation of one superradiant state (the one with the largest

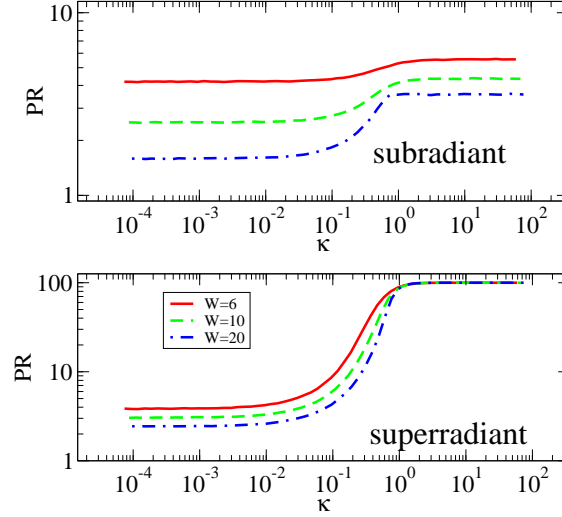


Figure 3.3: The participation ratio PR is shown as a function of κ for different disorder strengths. In the upper panel we consider states with $-1.5 \leq E/\Omega \leq -0.5$, which become subradiant for large κ , while in the lower panel we consider the state with the largest width, which corresponds to the superradiant state for large κ . Here $N = 100$, $\Omega = 1$, and the PR is averaged over 4000 disorder realizations.

width) and $N - 1$ subradiant ones. In Fig. 3.3 (upper panel) we analyze the PR as a function of κ for the subradiant states for $\kappa > 1$, and in Fig. 3.3 (lower panel) we analyze the case of the state with the largest width, which becomes superradiant for $\kappa > 1$. As the opening, determined by the parameter κ , increases, the PR of both superradiant and subradiant states increases, showing that the opening has a delocalizing effect. But the consequences of the opening are very different for superradiant and subradiant states. For the latter, the PR reaches a plateau value above the ST ($\kappa \approx 1$), which is slightly higher than the PR for $\kappa \ll 1$. Moreover on increasing the disorder, the PR of the subradiant states decreases, both below and above the ST, see Fig. 3.3 upper panel. The situation is different for the superradiant states. Above the ST these states become completely delocalized ($PR \approx N$) and the delocalization is not affected by an increase in W , see Fig. 3.3 lower panel.

We now look more closely at how the subradiant and superradiant states are affected differently by increasing the disorder strength W . In Fig. 3.4, we consider the case of $N = 100$ and $\gamma = \Omega = 1$. For small disorder we have $D \approx 4\Omega/N$, so that

$$\kappa = \gamma/D = \gamma N/4\Omega \approx 25 \gg 1.$$

This implies that we are in the superradiant regime. Moreover, for sufficiently small disorder, we have that the localization length is larger than the system size, $\xi \approx 100 \Omega^2/W^2 > N$, so that both superradiant and subradiant states are delocalized. For larger disorder (here $W > 1$) we enter the localized regime, for which $\xi < N$. In this regime the PR of the subradiant states decreases, while the PR of the superradiant state remains unchanged ($PR = N$), signaling a superradiant state that remains completely delocalized. As we increase disorder further, κ decreases according to Eq. (3.9). The ST occurs at $W \approx \gamma N$, here $W \approx 100$, and above this value the superradiance effect disappears. Summarizing, we have a critical value of disorder ($W \approx 100$ indicated as a full vertical line in Fig. 3.4) separating the superradiant regime ($\kappa > 1$), from the non-superradiant one ($\kappa < 1$). Only for $W > 100$, i.e., below the ST, the superradiant states begin to localize, and, for very large disorder, corresponding to very small κ , they behave in the same way as the subradiant states.

We also note that the subradiant states are affected by disorder as the eigenstates of the closed system in the delocalized superradiant regime. When $W > 1$ we enter in the localized superradiant regime and the differences between the subradiant modes and the eigenstates of the close system become considerable. This behavior can be viewed as a signature of the fact that the subradiant states are effectively decoupled from the external world and then they behave similarly to those of the closed system. For $W \ll 1$ the numerical simulation of the PR of the closed system reproduce the analytical prevision $PR = 2N/3$.

The regime for which the behavior of superradiant state and subradiant modes is strongly different is the *localized superradiant* regime. The value of W for

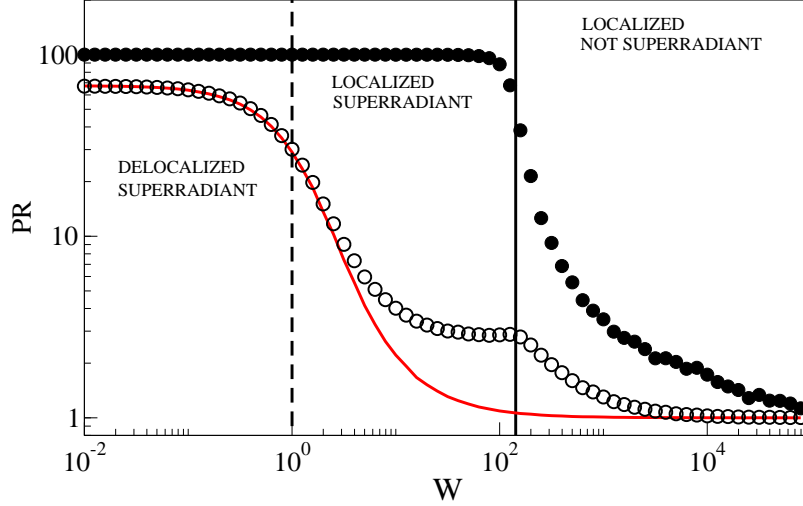


Figure 3.4: The participation ratio is shown as a function of the disorder strength W . Open circles stand for the subradiant states, full circles indicate the superradiant state, while the red line stand for the closed system. Each point is obtained by averaging over 100 disorder realizations for the superradiant state, while for the subradiant states, an additional average over all the subradiant states is performed. For the closed system we have averaged over all the states. The right and left vertical lines indicate the ST and the delocalization transition, respectively. Here $N = 100$ and $\gamma = \Omega = 1$.

which Anderson transition takes place depends on N because

$$\xi \approx N \implies W \approx \frac{10\Omega}{\sqrt{N}}. \quad (3.13)$$

Let us notice that the value of W for which superradiant transition takes place also depends on N . According to Eq.(3.9), in order to have $\kappa \simeq 1$, one should put

$$W \approx \gamma N \quad (3.14)$$

so that W have to increase linearly with N . This means that the range of W where the difference between the two subspaces is strong can be increased just increasing

N : in Figure 3.4 the localization transition threshold move to the left and the ST move to the right.

In this section we have focused our attention on the degree of localization of the eigenstates of \mathcal{H} mainly using the PR. In Figure 3.5 our results are summarized: the PR is shown as a function of the opening γ and of the disorder strength W/Ω for a fixed size of the chain.

Note that we use two different colors scale for the two panels in order to increase the visibility.

It is important to note that what was known is only the behavior of the PR for the closed Anderson model, i.e. on the W/Ω axis of the Figure 3.5. While here we have fully analyzed the whole $(W/\Omega, \gamma)$ plane.

3.5 Discussion

In this Section we will justify (using perturbation theory) and briefly discuss the interesting results presented previously: for small κ (below the ST) all the states are affected in a similar way by the opening and disorder, while for large κ (above the ST), the superradiant states remain completely delocalized, independently of the degree of disorder, while the subradiant states are still sensitive to disorder, and their PR decreases with increasing disorder.

3.5.1 Perturbative approach for $\kappa \ll 1$

In the limit $\kappa \ll 1$, the eigenstates of \mathcal{H} at first order in perturbation theory can be written as:

$$|n\rangle = \frac{1}{\sqrt{C_n}} \left[|n^0\rangle - i\frac{\gamma}{2} \sum_{k^0 \neq n^0} \frac{\langle k^0 | Q | n^0 \rangle}{E_{n^0} - E_{k^0}} |k^0\rangle \right], \quad (3.15)$$

where $|n^0\rangle$ are the eigenstates of the closed system, i.e., of the Anderson model. Of course, the perturbation expansion makes sense only when each coefficient in the sum in Eq. (3.15) is much less than one. This cannot be true, in general, since the eigenvalues E_{n^0} are random numbers uniformly distributed in the interval

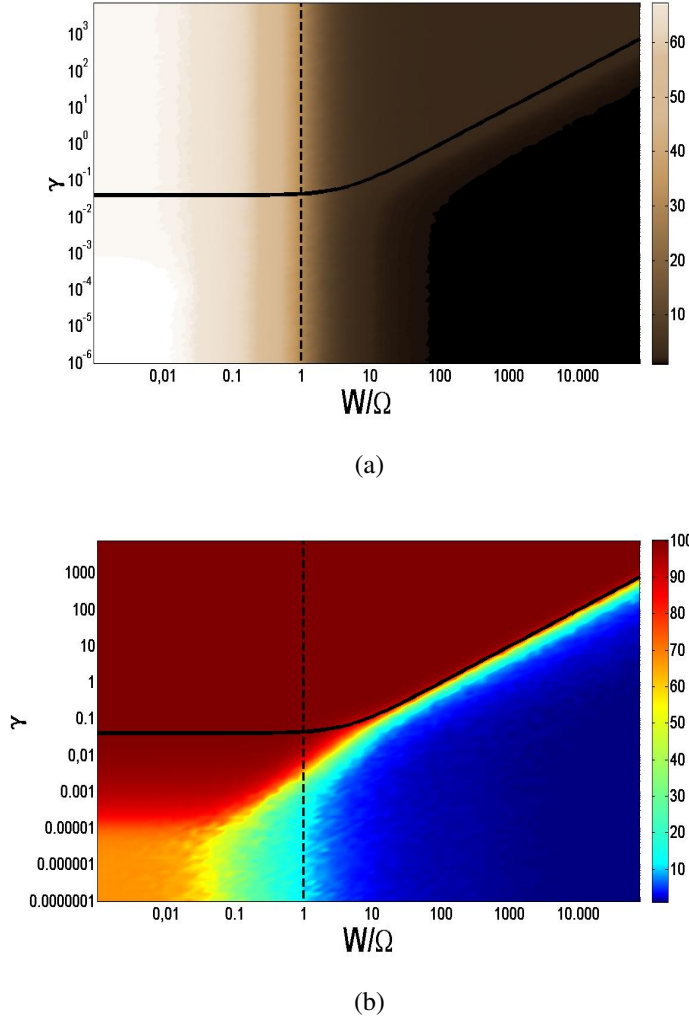


Figure 3.5: (a) PR of subradiant states as a function of γ and W/Ω ; (b) PR of superradiant states as a function of γ and W/Ω . In both cases $N = 100$. Each data set is obtained averaging over 10 realizations for the superradiant state while for the subradiant states an additional average over all the subradiant subspace has been done.

$[-W/2, W/2]$. Thus perturbation theory cannot be applied *tout court*, but only for those states whose energies are not too close one to each other.

This simple observation has deep consequences on the structure of the eigenstates. Indeed we observed numerically that on the one hand many single-peaked eigenstates become double- or multiple-peaked as γ increases, while on the other hand, they all develop a constant plateau proportional to $(\gamma/W)^2$. The secondary peak and their positions along the chain are not correlated and then if we average over the realization we obtain an *average probability distribution* which clearly show the plateau mentioned above, see Fig. 3.6. The physical meaning of the average probability distribution is discussed in subsection 3.6.1.

This last fact can be easily explained using first-order perturbation theory as given by Eq. (3.15): in the deep localized regime $W \gg \Omega$, the matrix elements $\langle k^0 | Q | n^0 \rangle$ are of order unity and the average distance between two random energies is $W/3$, so that the typical coefficients $\langle k_0 | n \rangle$ in Eq. (3.15) are $\sim \gamma/W$. Furthermore, the mean level spacing is $D \approx W/N$, and thus the few largest coefficients in Eq. (3.15) are typically $\sim \gamma N/W \sim \kappa$ (using Eq. (3.9)). Thus for weak opening ($\kappa \ll 1$), the *typical* eigenstate consists of a single Anderson model eigenstate with a $O(\kappa^2)$ admixture of other states, and therefore the *typical PR* for small κ differs only by $O(\kappa^2)$ from the *PR* of the Anderson model.

As already remarked previously, the perturbative approach cannot always work, because for arbitrarily small κ there is a small but finite probability that two energy states are too close together. This clustering behavior has important consequences for the localization properties. Specifically, since the nearest-neighbor level spacing distribution of uniform random numbers E_{n^0} is Poissonian: $P(s) = (1/D) e^{-s/D}$, where s is the energy difference between nearest-neighbor levels and $D = W/N$ is the mean level spacing, we can evaluate the probability to have two levels closer than $\gamma/2$ as $1 - e^{-\gamma/2D} \approx \kappa/2$ for small κ . This means that there are κN states out of N , for which perturbation theory cannot be applied. When this happens, the Anderson states mix strongly and the *PR* increases by an $O(1)$ factor. Thus, even though this behavior is rare, it makes an $O(\kappa)$ contribution to the *average PR* of the weakly open system, which exceeds the $O(\kappa^2)$ contribution

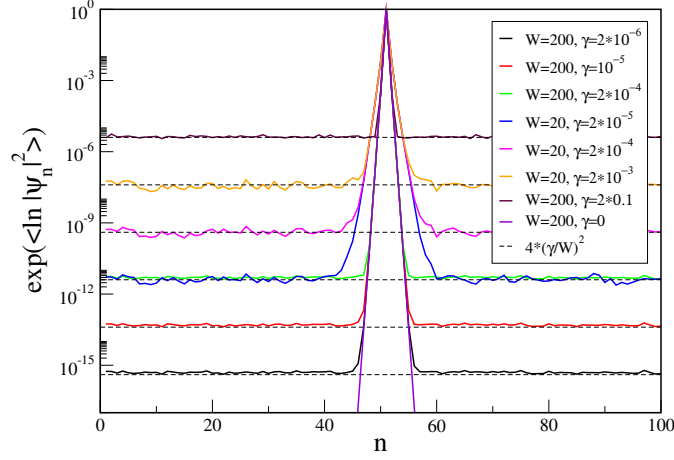


Figure 3.6: The averaged probability distribution of all eigenstates of the non-Hermitian Hamiltonian that are strongly peaked in the middle of the chain is shown for different coupling strength γ and disorder strength W , as indicated in the caption. Specifically, we average over all eigenstates having a probability > 0.9 at the site $n = N/2 + 1$ in order to avoid double-peaked states, and also average over disorder. Moreover, to reduce fluctuations, we average the logarithm of the probability distribution. In all cases we fix $N = 100$ and $\Omega = 1$. Dashed horizontal lines are proportional to $(\gamma/W)^2$ in agreement with the perturbative approach.

from the typical states. Indeed the average PR can be evaluated as follow:

$$PR = \frac{N\kappa PR_2 + (1 - \kappa)NPR_1}{N} = PR_1 + \kappa(PR_2 - PR_1)$$

where PR_1 and PR_2 refer to the PR of the states for which perturbation theory can and cannot be applied. Since $PR_1 \simeq PR(\gamma = 0) + O(\kappa^2)$, and $PR_2 \simeq O(1)$, we have that $PR(\gamma) - PR(\gamma = 0) \simeq \kappa$. The numerical results in Fig. 3.7 confirm that the effect of the opening on the PR grows as κ , instead of the κ^2 growth predicted by first-order perturbation theory. Here we present the average (over disorder) of $PR(\gamma) - PR(\gamma = 0)$, as a function of $\kappa = N\gamma/W$ for fixed disorder strength and different values of the system size. In any case this is quite a delicate point and we postpone its full analysis to a future work.

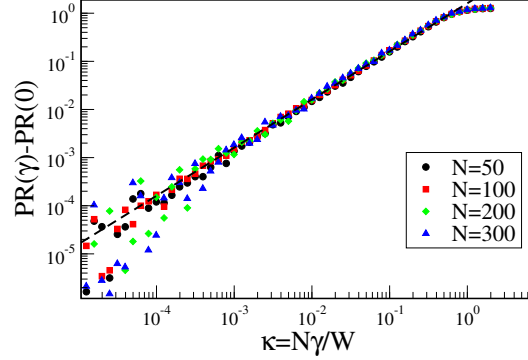


Figure 3.7: The average increase in the participation ratio, compared with the closed system, is calculated as a function of κ , for fixed disorder $W = 20$ and different system sizes N as indicated in the legend. In each case the average is performed over 50000 different eigenstates. The line is $PR(\gamma) - PR(0) = 2\kappa$.

3.5.2 Perturbative approach for $\kappa \gg 1$

In the limit $\kappa \gg 1$ we consider two cases. First, we consider the situation where the nearest neighbor tunneling coupling is $\Omega = 0$, in which case we can follow the approach explained in Ref. [18]. This approach will be very useful also for the case $\Omega \neq 0$, which we treat here below.

$\Omega = 0$ and $\kappa \gg 1$

If $\Omega = 0$ the Anderson Hamiltonian is diagonal in the site basis $|j\rangle$ with eigenvalues E_j distributed uniformly in the interval $[-W/2, W/2]$. The eigenstates of the non-Hermitian part $-i\frac{\gamma}{2}Q$ of the effective Hamiltonian are $|d\rangle = \frac{1}{\sqrt{N}}(1, \dots, 1)^T$ (the superradiant state) with eigenvalue $-i\frac{\gamma}{2}N$, and $N - 1$ degenerate eigenstates $|\mu\rangle$ with eigenvalue 0 (the subradiant states). We will choose $|\mu\rangle$ in a convenient manner later. Following Ref. [18] we can rewrite \mathcal{H} in the basis of these eigenstates using the transformation matrix V , which has as its columns the eigenstates of Q :

$$\tilde{\mathcal{H}} = V^T H_0 V - i\frac{\gamma}{2} V^T Q V = \begin{pmatrix} -i\frac{\gamma}{2}N & \vec{h}^T \\ \vec{h} & \tilde{H} \end{pmatrix}. \quad (3.16)$$

Here \vec{h} is a vector of dimension $N - 1$ with components

$$h_\mu = \frac{1}{\sqrt{N}} \sum_{j=1}^N E_j \langle j | \mu \rangle, \quad (3.17)$$

while the matrix elements of the $(N - 1) \times (N - 1)$ submatrix \tilde{H} are

$$\tilde{H}_{\mu\nu} = \sum_{j=1}^N E_j \langle \mu | j \rangle \langle j | \nu \rangle. \quad (3.18)$$

Now, we can diagonalize \tilde{H} ,

$$\tilde{H}_{\mu\nu} = \sum_{j=1}^N E_j \langle \mu | j \rangle \langle j | \nu \rangle = \langle \mu | H_0 | \nu \rangle = \tilde{\epsilon}_\mu \langle \mu | \nu \rangle. \quad (3.19)$$

Following Ref. [18] we obtain

$$|\mu\rangle = h_\mu \frac{1}{\tilde{\epsilon}_\mu - H_0} |d\rangle = \frac{h_\mu}{\sqrt{N}} \sum_{j=1}^N \frac{1}{\tilde{\epsilon}_\mu - E_j} |j\rangle, \quad (3.20)$$

where the normalization coefficients h_μ are given by

$$h_\mu = \left(\langle d | \frac{1}{(\tilde{\epsilon}_\mu - H_0)^2} | d \rangle \right)^{-1/2}. \quad (3.21)$$

In the limit $\kappa \gg 1$, the eigenstates $|\mu\rangle$ of the non-Hermitian part of \mathcal{H} are also eigenstates of \mathcal{H} . Since $\langle d | \mu \rangle = 0$ we have,

$$\sum_{j=1}^N \frac{1}{\tilde{\epsilon}_\mu - E_j} = 0. \quad (3.22)$$

Therefore each eigenvalue of \tilde{H} lies between two neighboring levels E_n , so that the values $\tilde{\epsilon}_\mu$ are also confined in the interval $[-W/2, W/2]$.

Let us now estimate the magnitude of the mixing matrix elements h_μ . To do this we compute

$$\vec{h} \cdot \vec{h} = \frac{1}{N} \sum_{\mu=1}^{N-1} \sum_{i=1}^N \sum_{j=1}^N E_i E_j \langle \mu | i \rangle \langle j | \mu \rangle, \quad (3.23)$$

and using the completeness relation $\sum_{\mu=1}^{N-1} \langle j | \mu \rangle \langle \mu | i \rangle = \langle j | i \rangle - 1/N$ we have

$$\vec{h} \cdot \vec{h} = \langle E^2 \rangle - \langle E \rangle^2 = \Delta E^2. \quad (3.24)$$

This leads to

$$|h_\mu| \sim \frac{\Delta E}{\sqrt{N-1}} = \frac{W}{\sqrt{12(N-1)}}. \quad (3.25)$$

Each eigenstate $|\mu\rangle$ in Eq. (3.20) is a superposition of all the site states $|j\rangle$ with amplitudes $\frac{h_\mu}{\sqrt{N(\tilde{\epsilon}_\mu - E_j)}} \sim \frac{W}{N(\tilde{\epsilon}_\mu - E_j)}$ that depend only on the energies E_j and not on the site positions j . Nevertheless, each state $|\mu\rangle$ is quite localized, since the amplitudes are of order unity for the $O(1)$ number of sites whose energy is within a few mean level spacings of $\tilde{\epsilon}$ (i.e., when $|\tilde{\epsilon}_\mu - E_j| \sim D = W/N$), and small otherwise. This small value of the PR for the subradiant states should be compared with $PR = N$ of the superradiant states.

The values obtained above for the subradiant and the superradiant states correspond to zeroth-order perturbation theory. On the other hand first-order perturbation theory gives:

$$\begin{aligned} |SR\rangle &= \frac{1}{\sqrt{C}} \left[|d\rangle + \frac{W}{\sqrt{12(N-1)}} \sum_{\mu=1}^{N-1} \frac{r_\mu}{-i\frac{\gamma}{2}N - \tilde{\epsilon}_\mu} |\mu\rangle \right] \\ &= \frac{1}{\sqrt{C}} \left[|d\rangle - \frac{1}{\kappa \sqrt{3(N-1)}} \sum_{\mu=1}^{N-1} \frac{r_\mu}{i + 2\tilde{\epsilon}_\mu/\gamma N} |\mu\rangle \right] \\ |SUB_\mu\rangle &= \frac{1}{\sqrt{C'_\mu}} \left[|\mu\rangle + \frac{W}{\sqrt{12(N-1)}} \frac{r_\mu}{\tilde{\epsilon}_\mu + i\frac{\gamma}{2}N} |d\rangle \right] \\ &= \frac{1}{\sqrt{C'_\mu}} \left[|\mu\rangle + \frac{1}{\kappa \sqrt{3(N-1)}} \frac{r_\mu}{i + 2\tilde{\epsilon}_\mu/\gamma N} |d\rangle \right], \end{aligned} \quad (3.26)$$

where r_μ are random coefficients with $\langle r_\mu^2 \rangle = 1$. We see that the exact superradiant state $|SR\rangle$ is a combination of the unperturbed superradiant state $|d\rangle$ and a small admixture of the unperturbed subradiant states $|\mu\rangle$, and the mixing probability decreases as $1/\kappa^2$ for large κ . Similarly, the admixture of the unperturbed superradiant state $|d\rangle$ in each exact subradiant states $|SUB_\mu\rangle$ decreases as $1/(\kappa^2 N)$. This shows that $PR \approx N$ for the superradiant state and $PR \sim 1$ for the subradiant states when $\kappa \gg 1$.

$\Omega \neq 0$ and $\kappa \gg 1$

As a first step we write the Anderson Hamiltonian H_0 in terms of its eigenstates $|n\rangle$. Obviously the form of $|n\rangle$ will depend on the degree of disorder W . In the following we limit our considerations to the large disorder regime, so that in the basis of the eigenstates of H_0 , the matrix elements of Q remain of order one, $Q_{nm} \sim 1$, and we can use the results of Sec. 3.5.2, with the site states and energies $|j\rangle$ and E_j replaced by the Anderson eigenstates and eigenenergies $|n\rangle$ and E_n .

In Fig. 3.4 we see that for $\kappa > 1$ (corresponding to $W < 100$), the superradiant state remains unaffected by the increase of disorder, while the subradiant states become more localized as the disorder strength is increased. The results of the previous section can be used to understand this strongly asymmetric behavior of the PR between the subradiant states and the superradiant state. Indeed at zeroth order in perturbation theory we can see that the superradiant state $|SR\rangle \approx |d\rangle$ is completely delocalized, $PR = N$, while subradiant states $|SUB_\mu\rangle \approx |\mu\rangle$ become more and more localized as we increase disorder. Specifically, the site states $|j\rangle$ in Eq. (3.20) are replaced with Anderson eigenstates $|n\rangle$, with localization length $\xi \propto 1/W^2$. This difference persists in first-order perturbation theory, since the mixing probability between the super- and sub-radiant states decreases as $1/\kappa^2$ for large κ , see Eq. (3.26).

Our perturbative approach justifies the results presented in Fig. 3.4, where we can see that the subradiant states become increasingly localized as we increase disorder. At the same time Fig. 3.4 shows that the superradiant state remains completely delocalized on increasing W , until we reach the value $W \approx 142.8$ ($\kappa = 0.7$) where we find numerically that the ST takes place. The perturbative approach shows that superradiant states are much less sensitive to disorder because their complex energies are at a distance greater than $\gamma N/2 = W\kappa/2$ from the subradiant states.

3.6 Further results

3.6.1 Structure of the averaged probability distribution in large disorder limit

In this subsection we show some preliminary results on the structure of the *averaged probability distribution* (APD) of the eigenstates for $W/\Omega \gg 1$ in the limit of small ($\kappa \ll 1$) and large ($\kappa \gg 1$) opening.

We recall that if ψ is a wave function, the averaged probability distribution is defined as $\langle |\psi|^2 \rangle$, where the symbol $\langle \dots \rangle$ stand for the average over different random realizations.

Sometimes, in order to reduce fluctuations, we made a logarithmic average, i.e. $\exp(\langle \ln \psi \rangle)$, instead of the standard average.

The two different average method, classical and logarithmic, can give generally different results. Is important to note that if ψ is normalized the APD is normalized too only if a classical average is made, otherwise it is not.

The study of the APD is very important because it is a quantity which can be measured experimentally. In some interesting recent papers, see for example [25, 26], the diffusion of a non-interacting Bose-Einstein condensate, in a one-dimensional disordered potential is measured in order to study Anderson localization. The quantity measured in this kind of experiments is the spatial distribution of the atomic density (number of atoms / μm). If the particles that constitute the condensate are non-interacting then the APD can be related to the atomic density profile.

As we have shown in Figure 3.6, in the limit $\kappa \ll 1$ and $W/\Omega \gg 1$, the APD of the eigenstates peaked in a certain site, consists of two terms: the APD of the closed Anderson model and a plateau proportional to $(\gamma/W)^2$ and independent of N . This result can be explicitly deduced using first-order perturbation theory, see Eq.(3.15).

In the opposite limit, $\kappa \gg 1$ and $W/\Omega \gg 1$, we have found a very similar APD for the eigenstates of \mathcal{H} . In this regime, the APD of the eigenstates peaked in the middle of the chain consists of two terms: the APD of the closed Anderson model

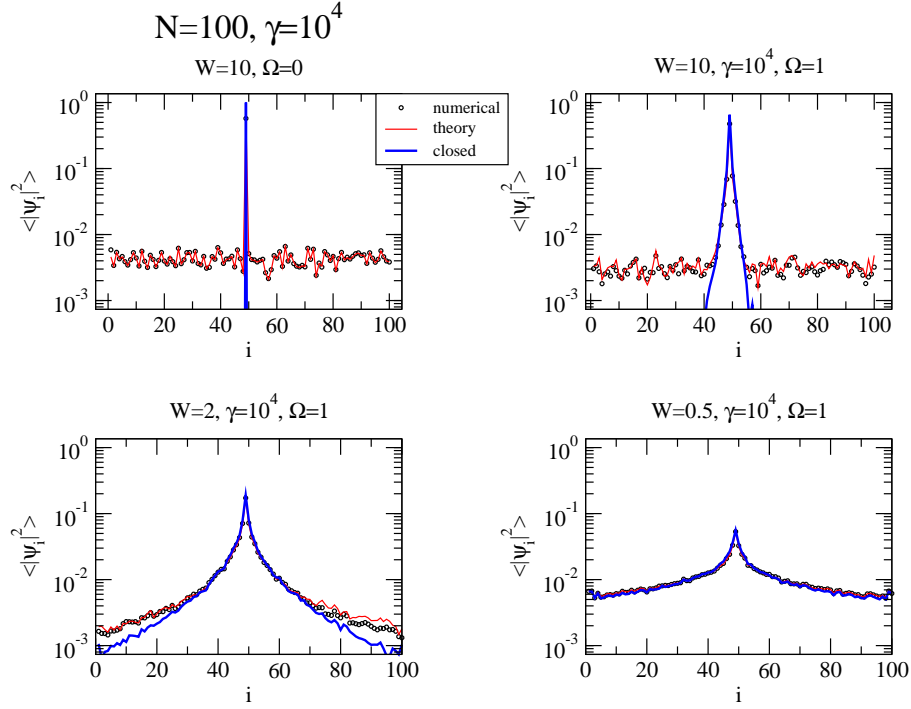


Figure 3.8: Comparison between perturbative formula (3.20) and numerical results for different W . Here an average over 10^3 disordered configuration is made.

and a plateau proportional to $1/N$ (and independent of γ and W).

Also in this case first-order perturbation theory can predict the structure of the wave function in $\kappa \gg 1$ limit, see Eq.(3.20). Even if we have not been able to deduce explicitly the value of the plateau from Eq.(3.20) we have checked numerically that Eq.(3.20) can reproduce the structure of the eigenstates in this limit, see Figure 3.8. It is important to note that Eq.(3.20) correspond to zero-th order expansion of the subradiant eigenstates of \mathcal{H} . In principle Eq.(3.20) is valid in the large disorder limit, however from Figure 3.8 we can see that it is valid also for $W = 2$ and $W = 0.5$.

A comparison between these two structures is shown in Figure 3.9. In this figure we can also compare the results of the two different kind of average, classical and logarithmic.

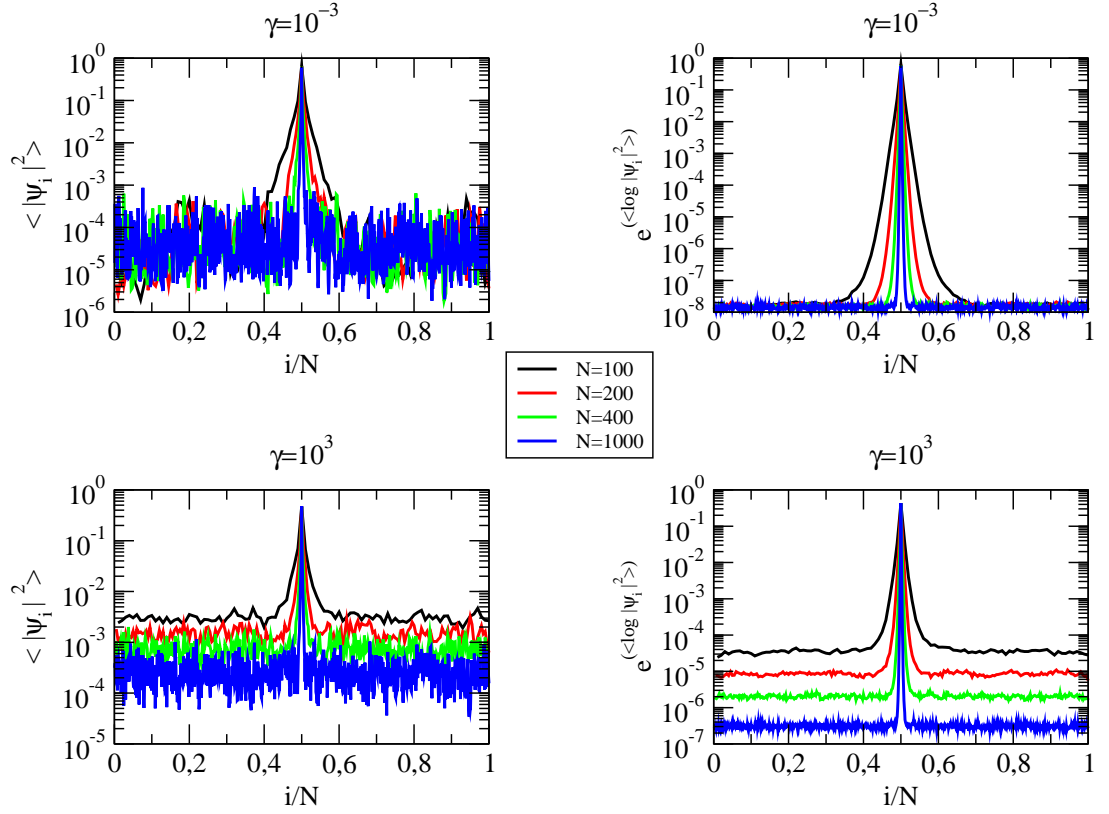


Figure 3.9: In the upper panels we compare the two kinds of average in the limit $\kappa \ll 1$ and $W/\Omega \gg 1$. In this case the plateau are independent of N and so the averages give the same result: the plateau does not scale with N , but we note also that the absolute value of the plateau is different. In the lower panels we compare the two average in the limit $\kappa \gg 1$ and $W/\Omega \gg 1$. We can see that in the case of classical average the plateau scale as N while in the case of logarithmic average the plateau scale as N^2 . Here we have set $W = 10$ and we average over 10^3 configuration.

In the large disorder limit the localization length is $\xi \approx 1$. For this reason, if we compute the APD (from a classical average) of the eigenstates peaked in the middle of the chain, $|\psi\rangle$, the normalization condition for the APD can be written as

$$A + (N - 1)B = 1, \quad (3.27)$$

where $A = \langle |\psi_{N/2}|^2 \rangle$ and $B = \langle |\psi_i|^2 \rangle$ with $i \neq N/2$. Of course here A and B are the values of the APD of the top of Anderson peak and of the plateau respectively.

As a consequence of Eq.(3.27), the different behavior of the plateau in the regimes discussed above implies a different behavior of the Anderson peak. In fact from Eq.(3.27) is possible to deduce that

$$A = 1 - (N - 1)B. \quad (3.28)$$

In the $\kappa \ll 1$ limit, we have $B \approx \beta(\gamma/W)^2$ and then for large N ,

$$A \approx 1 - \beta N \left(\frac{\gamma}{W} \right)^2. \quad (3.29)$$

In the $\kappa \gg 1$ limit, we have $B = \alpha/N$ and then for large N ,

$$A \approx 1 - \alpha. \quad (3.30)$$

Here α and β are two constants.

Summarizing the coefficients A and B have to respect the relation

$$\begin{aligned} \kappa \ll 1 \implies A &\approx 1 - \beta N (\gamma/W)^2 \\ B &\approx \beta (\gamma/W)^2 \\ \kappa \gg 1 \implies A &\approx 1 - \alpha \\ B &\approx \alpha/N. \end{aligned} \quad (3.31)$$

In Figure 3.10 we have compared Eqs. (3.31) with the numerical results. The coefficients α and β are obtained fitting the data relative to B , see upper panels. From the fit of numerical results we obtain

$$\alpha \approx 0.43$$

$$\beta \approx 3.7 \cdot 10^5. \quad (3.32)$$

The theoretical previsions 3.31 are not in agreement with the numerical results for the A coefficients in the limit of small coupling ($\kappa \ll 1$). This discrepancy arise from the rough approximation of the APD, see Eq(3.27). In order to avoid this problem a more accurate description of the APD is needed: we have to take into account the exponential shape of the Anderson peak.

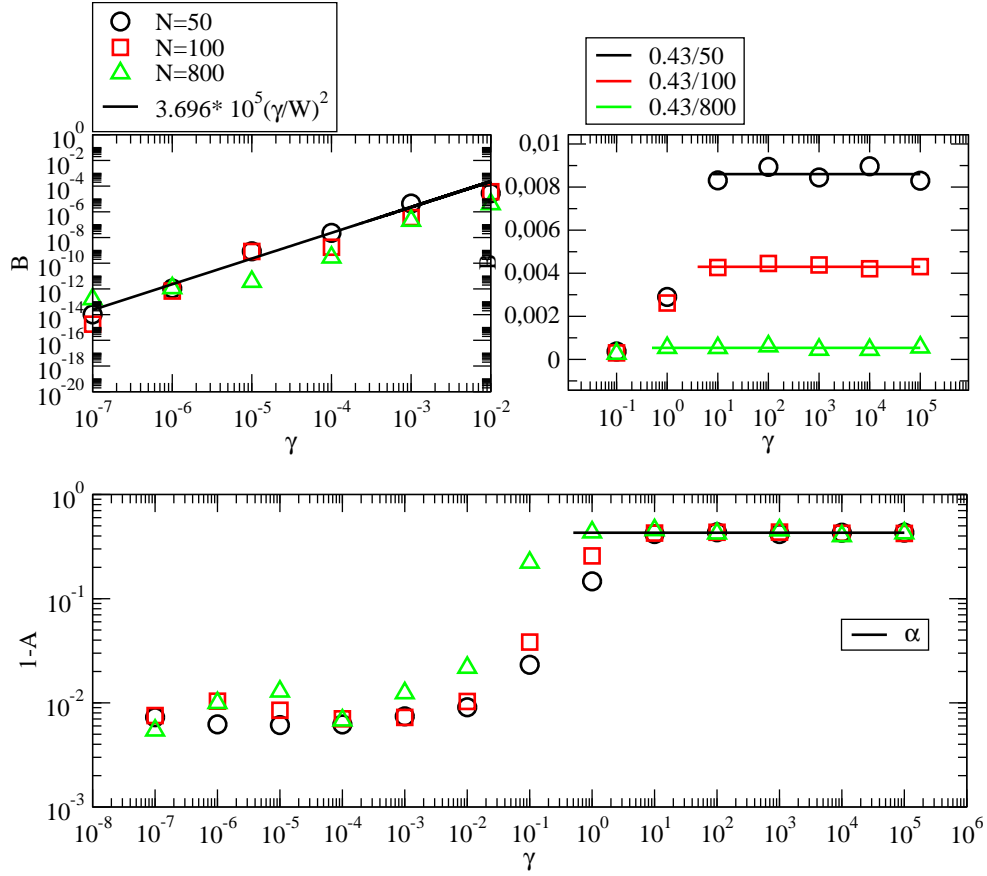


Figure 3.10: Upper panels: B as a function of γ . Lower panels: $1 - A$ as a function of γ . Left figures are for $\kappa \ll 1$ while right are for $\kappa \gg 1$. The symbols are the numerical results while the solid lines are Eqs. (3.31). The free parameters α and β are obtained fitting the data relative to B and used to compute the theoretical formulae for $1 - A$. Each point is obtained averaging over 10^3 realization for $N = 50$, 100 realization for $N = 100$ and 10 realization for $N = 800$. Here $W/\Omega = 400$. For each value of N the ST takes place for a different value of γ , see Eq. (3.9). In the right upper panel, the horizontal solid lines, starts for $\kappa = 1$.

In Figure 3.11 we focus our attention on the plateau, B . Here B is plotted as a function of γ for $W = 40$ and different size of the chain.

From this figure we clearly note that the ST is approximatively the threshold where we have a discontinuity in the plateau behaviors. This is not trivial because

we have considered only the cases $\kappa \ll 1$ and $\kappa \gg 1$ and in principle we do not know the behavior of A and B for intermediate values of κ . The results confirm that, when a logarithmic average is made, the plateau increase as $B \approx 4(\gamma/W)^2$ for $\kappa \ll 1$ while for $\kappa \gg 1$ the scaling law is $B \propto 1/N^2$.

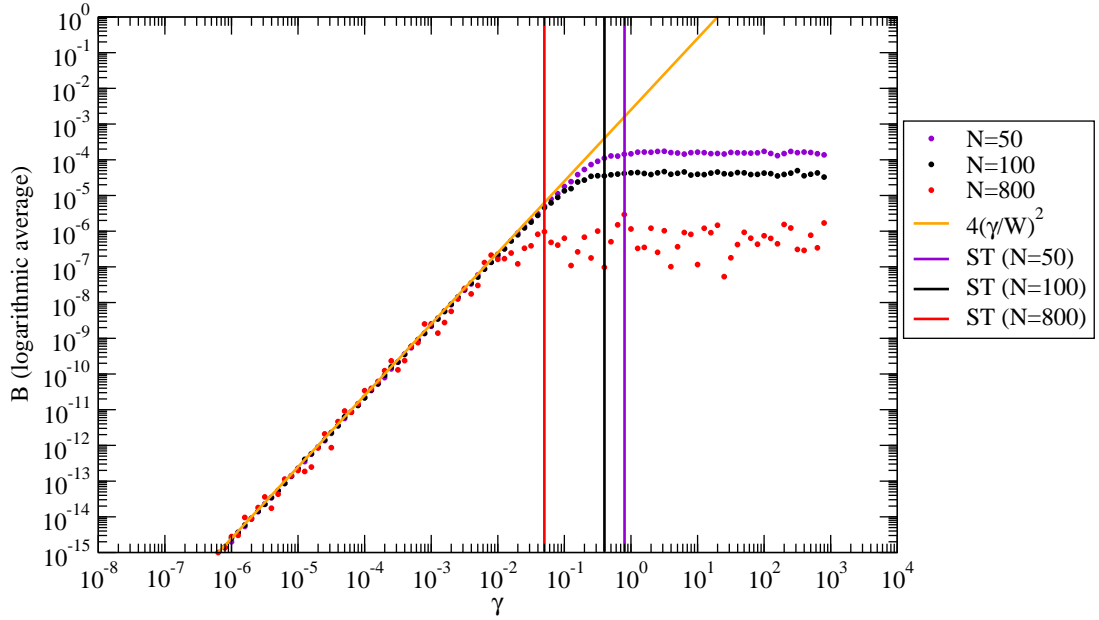


Figure 3.11: B as a function of γ . The circles are the numerical results while the solid lines are the theoretical prevision. Each point is obtained averaging over 10^3 realization for $N = 50$, 100 realization for $N = 100$ and 10 realization for $N = 800$. Here $W/\Omega = 40$. The vertical solid line are the STs for different N , the colors reflect the different numerical data.

3.6.2 Conductance

In order to understand how the opening affects the transport propeties of the system we have studied the conductance. The modified model used to compute the

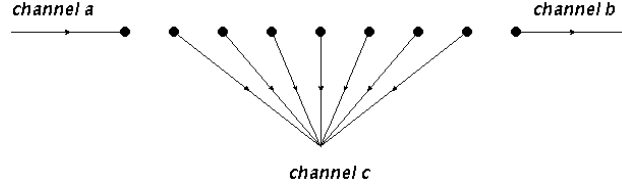


Figure 3.12: Modify model used to compute the conductance.

conductance is shown in Figure 3.12. The edge state on the left, 1, is coupled to channel a with coupling strength γ_a , the edge state on the right, N , is coupled to channel b with coupling strength γ_b , and the sites in the middle, between 2 and $N - 1$, are coupled to a common channel c with coupling strength γ_c . In this framework one should treat the a -channel and the b -channel as *left* and *right* channels corresponding to incoming and outgoing waves respectively. The conductance from a to b channel is given by the adimensional Landauer formula [19, 23] in the standard way

$$\begin{aligned} G(E) &= \mathsf{T}^{ab}(E) \\ &= |\mathcal{T}^{ab}(E)|^2, \end{aligned} \quad (3.33)$$

where \mathcal{T} is the transmission matrix defined in Eq.(1.30). In Figure 3.13 we have computed the behavior of G in function of the disorder strength W in the limit $\kappa \ll 1$.

We can see that if the system is not coupled to the common decay channel the conductance decreases as the the disorder increases. That makes sense because as W is increased the eigenstates became more and more localized and so the transport from channel a to channel b is inhibited. Otherwise if we switch on the coupling γ_c we note that a critical amount of disorder W_c exists, such that, for $W < W_c$, G behaves in the same way as for a closed system.

From the expression of the eigenstates of \mathcal{H} for small κ , see Eq. (3.15), we can in principle estimate the value of N , W or γ for which the effect of the

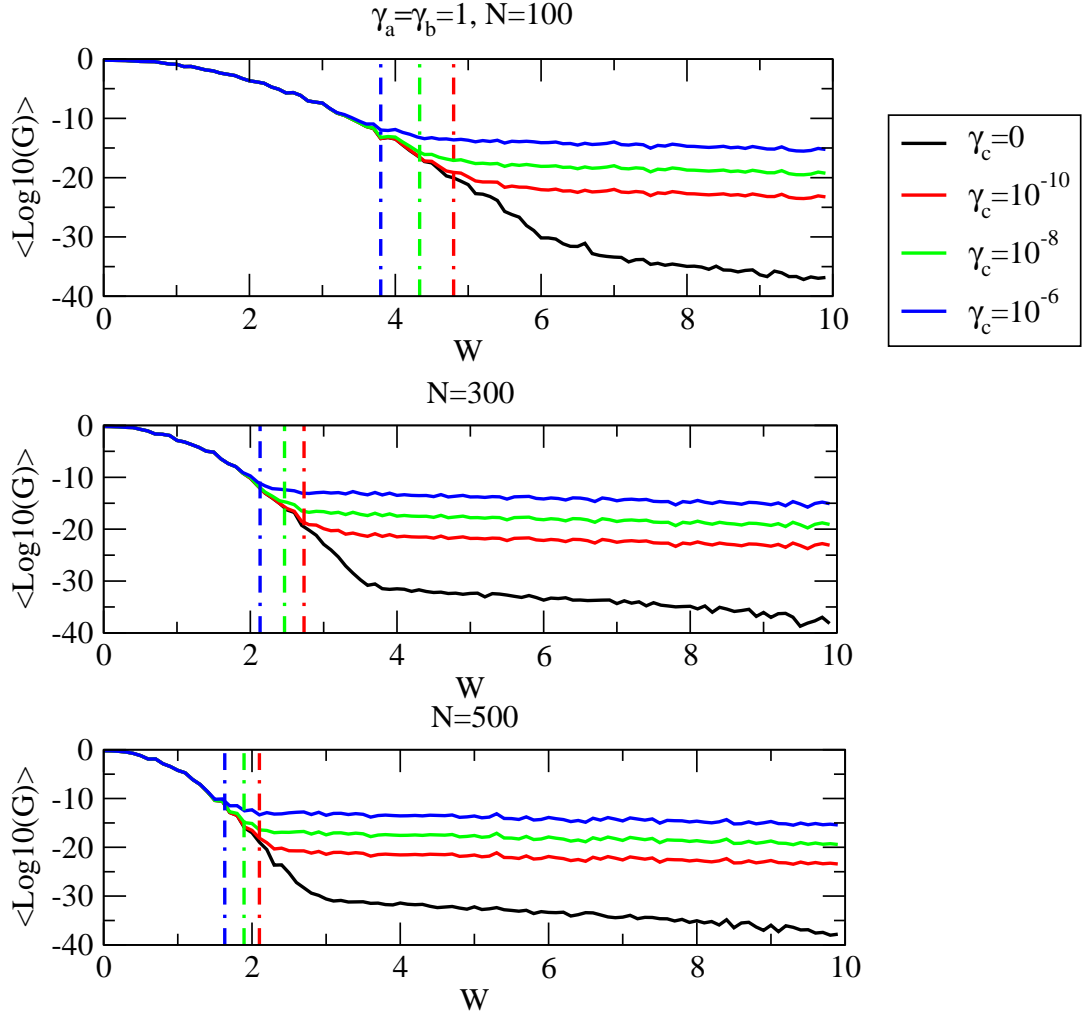


Figure 3.13: $\langle \log G(E=0) \rangle$ vs W for different values of the coupling strength to common decay channel γ_c and for different values of N as indicated in the legend. Here we average over 100 disorder configurations for $N = 100$ and over 50 configurations for $N = 300$ and $N = 500$. The coupling strength with edge channels is set $\gamma_a = \gamma_b = 1$. The dashed vertical line represents the critical value W_c , provided by the criterium (3.34), for which the system becomes sensitive to opening, i.e. the behavior is different from the closed Anderson model. The value provided by the above criterium have to be rescaled by the factor $3/2$.

long range coupling becomes important. Indeed, as we increase N or W , the wave function becomes localized, $|\psi(j)| \sim \exp(-|j - j_0|/\xi)$. The probability to be at the edge sites for a state localized in the middle of the chain goes like $\exp(-N/\xi)$, with $\xi \sim 105.2/W^2$. On the other side from the Eq.(3.15) we have that for the coupling to the common channel the probability to find a state in one site is proportional to $(\gamma/W)^2$. So we can set the criterion:

$$\exp(-N/\xi) \approx \alpha \left(\frac{\gamma_c}{W} \right)^2, \quad (3.34)$$

where α is the proportionality constant. From Eq.(3.34) we are able to deduce W_c . This rough criterium provide us a value of W_c which is in good agreement with the numerical results for different value of N and γ_c as shown in Figure 3.13.

3.7 Conclusions

We have studied the 1D Anderson model with all sites coupled to a common decay channel (coherent dissipation). Our main motivation was to understand the interplay of opening and disorder. Increasing the disorder tends to localize the states. Increasing the opening, on the other hand, reduces the degree of localization, and in particular induces a superradiance transition, with the formation of a subradiant subspace and a superradiant state completely delocalized over all sites. Our results show that, while for small opening all the states tend to be similarly affected by the disorder, for large opening the superradiant state remains delocalized even as the disorder increases, while the subradiant states are much more affected by disorder, becoming more localized as the disorder increases. We have explained these effects qualitatively, mainly guided by perturbation theory. Indeed we have shown that the superradiant state is not affected by disorder, up to a critical disorder strenght for which the superradiance effect disappears. This is because its energy is very distant, in the complex plane, from the energies of the subradiant states.

There are different experiments [25, 26] about the localization of matter waves or light waves which can confirm the findings presented in this chapter.

Another important reason that drives us to study more this model is that, as we will show in the next chapter, we have found the same interesting features in the three-dimensional Anderson model with coherent dissipation and also in a cold atoms system [11]. This means that the 1D system is a really paradigmatic model and a powerful tool in order to understand the interplay of superradiance and disorder.

Chapter 4

Interplay of superradiance and disorder in the 3D Anderson model

In analogy with the one-dimensional case we want to study a 3D Anderson model in presence of coherent dissipation, i.e. when the particle can escape from the system at any site of the cubic lattice.

As in the case considered in Chapter 3, we have only one decay channel and all the couplings strength are equal. The effective Hamiltonian is given by

$$\mathcal{H} = H_0 - i\frac{\gamma}{2}Q, \quad (4.1)$$

Here, H_0 , is the standard Anderson Hamiltonian similar to (2.1) and $Q_{ij} = 1 \forall i, j$. The eigenvalues of \mathcal{H} are labelled as follow

$$\mathcal{E}_r = E_r - \frac{i}{2}\Gamma_r. \quad (4.2)$$

Compared with the closed system the main difference with respect to the 1D case is that here we have a critical value of the disorder strength for which all the eigenstates are exponentially localized, see chapter 2. For a tight binding model with diagonal uncorrelated disorder we have [20]

$$\frac{W_c}{\Omega} \approx 16.5. \quad (4.3)$$

Let us analyze the interplay of superradiance and disorder, similar to what it has been done for the 1D case, see Chapter 3.

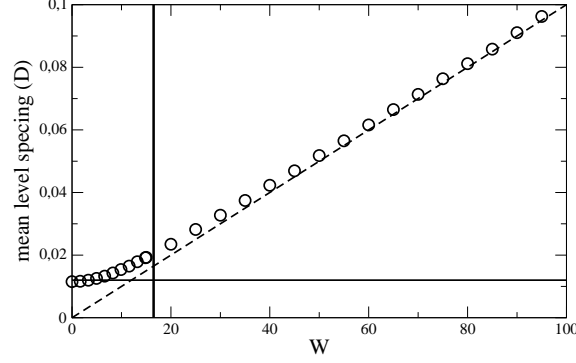


Figure 4.1: The mean level spacing, D , as a function of W for the closed system. Here $N = 10^3$, $\Omega = 1$ and each point is obtained averaging over 10 realizations. The horizontal solid line is $D = 12\Omega/N$, the dashed line is $D = W/N$ and the vertical solid line is the Anderson transition ($W = 16.5$).

4.1 Transition to superradiance

First of all let us show that, in this system, ST takes places after a certain value of coupling to the common decay channel.

The ST is expected to occur for $\langle \Gamma \rangle / D \approx 1$. The average width is γ and so

$$\kappa = \gamma/D, \quad (4.4)$$

is the effective coupling strength to the continuum. The mean level spacing as a function of the disorder strength is shown in Figure 4.1.

For small disorder the mean level spacing is given by $D \approx 12\Omega/N$ while for large disorder we have $D \approx W/N$ and then

$$\kappa \approx \frac{\gamma N}{W}. \quad (4.5)$$

In Fig. 4.2 we show that ST occurs at $\kappa \simeq 1$ for different values of W/Ω and N .

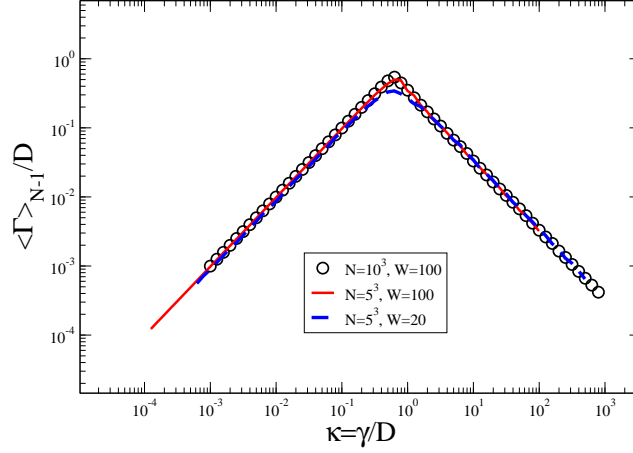


Figure 4.2: The average width of the $N - 1$ subradiant states, normalized by the mean level spacing D , versus the effective coupling strength κ for different values of N and W , and $\Omega = 1$. Here we averaged over 10 disordered configurations.

4.2 Sensitivity to disorder

In the paradigmatic 1D model we have found that subradiant and superradiant subspace are affected by the disorder in a different way. Subradiant states are sensitive to Anderson localization, like the eigenstates of the closed system, while the superradiant state is unaffected up to the superradiance transition. In order to study whether such a behavior occurs also in the 3D Anderson model we have computed the PR , defined in Eq.(3.7), as a function of disorder. The numerical results are shown in Figure 4.3.

In order to show how the disorder affects the superradiant and the subradiant subspaces, in Figure 4.3 we analyze both the participation ratio of the eigenstates of the effective Hamiltonian (PR), see Eq. (3.7), and the average decay widths, see Eq. (1.47).

Since in our model there is only one decay channel we have only one superradiant state and $N - 1$ subradiant states.

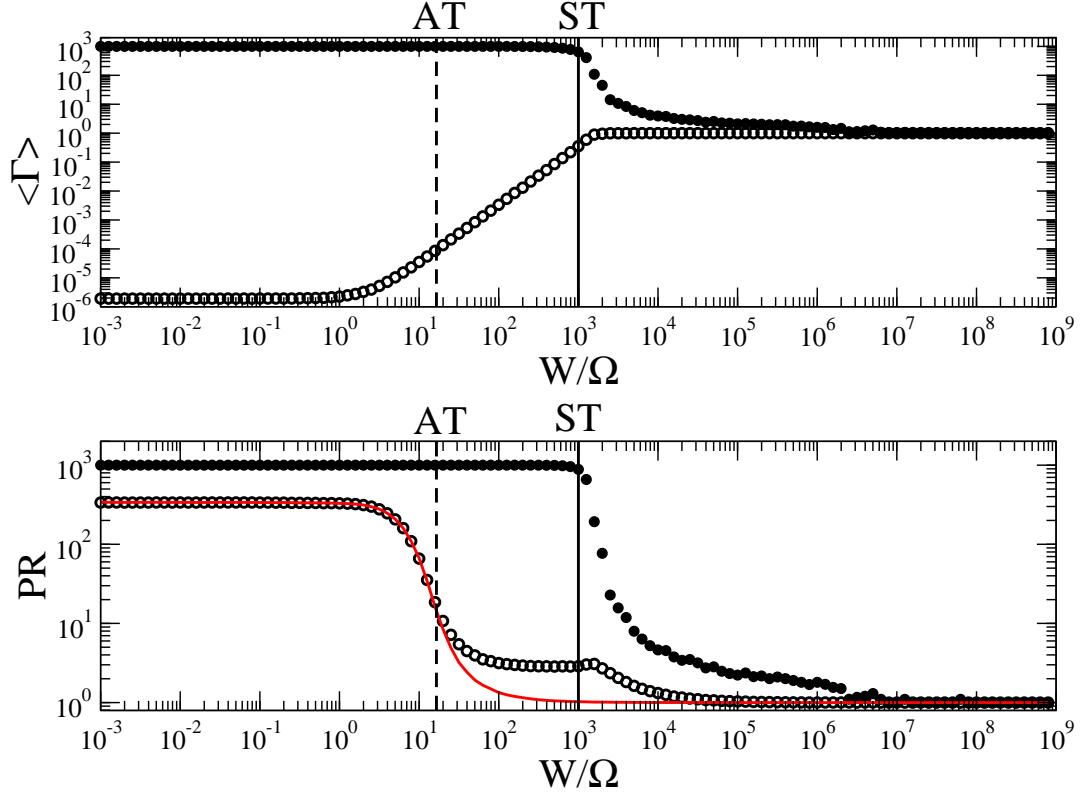


Figure 4.3: Upper panel: the average width versus W/Ω . Lower panel: the participation ratio is shown as a function of the disorder strength W/Ω . In both cases open circles stand for the subradiant states, full circles indicate the superradiant state, while the red line stand for the closed system. Each point is obtained by averaging over 10 disorder realizations for the superradiant state, while for the subradiant states, an additional average over all the subradiant states is performed. For the closed system we have averaged over all the states. The right and left vertical lines indicate the superradiance transition (ST) and the Anderson transition (AT), respectively. Here the system was a cube of $10 \times 10 \times 10$ sites ($N = 10^3$) and $\gamma = \Omega = 1$.

For each disorder strength we consider an average over 10 realizations for the superradiant state, while for the subradiant states, an additional average over all the subradiant states is performed.

We have chosen γ such that for small disorder, $W \ll 1$, we are in deep superradiant regime, i.e. $\kappa = \gamma/D \gg 1$. Increasing W we reach the Anderson transition threshold ($W \approx 16.5$), see the dashed vertical line in Figure 4.3. Above this critical value all the eigenstates of the closed model are exponentially localized but we are still in the superradiant regime.

If we increase the disorder strength further the mean level spacing increases as we have shown in Figure 4.1, and for large disorder the mean level spacing becomes proportional to W . Since the coupling to the continuum behaves as described by Eq.(4.5), for $W > \gamma N$ the superradiant effect disappears because $\kappa < 1$.

Summarizing, increasing W from $W \ll 1$ to $W \gg 1$, we span three different regimes labeled as: *delocalized superradiant* regime for ($W < 16.5$), *localized superradiant* regime (for $16.5 < W < \gamma N$), and *localized not superradiant* regime for ($W > \gamma N$). Note that for $W < 16.5$, the eigenstates of the closed system can be localized or not, depending on their energy eigenvalue, see discussion in Chap 2, while for $W > 16.5$ all the states of the closed system are localized.

In the lower panel the PR is plotted as a function of W . Here also the PR of the closed system is shown, see the red line. For the closed system we have averaged over all the eigenstates.

In the delocalized superradiant regime the superradiant state is fully delocalized ($PR = N$) and the subradiant states are extended as the eigenstates of the closed model.

If we increase W we cross the Anderson transition threshold and we enter in the localized superradiant regime. The PR of the subradiant states starts to decrease while the superradiant is not affected by this transition and it remains completely delocalized.

If W is increased further we enter in the localized not superradiant regime. Only above this critical value the superradiant state starts to localize and, only for very large disorder (corresponding to very small κ), they behave in the same way

as the subradiant states.

We also note that the subradiant states are affected by disorder as the eigenstates of the closed system in the delocalized superradiant regime, i.e. for $W < 16.5$. This behavior can be viewed as a signature of the fact that the subradiant states are effectively decoupled from the external world and therefore similar to the states of the closed system.

In the upper panel we show the average decay width of the subradiant and superradiant states. In the localized superradiant regime the average width of the superradiant states is approximately γN , while the average width of the subradiant states is very small. Here the average width of the two subspaces are well separated, signalling that we are in the superradiant regime.

When we enter in the localized superradiant regime the average width of the subradiant states starts to increase reaching the constant value γ while the average width of the superradiant state remains basically the same. Also in this regime the average width of the two subspaces are segregate but we can see that the disorder tends to destroy the subradiant states. Finally, when the disorder is such that $\kappa < 1$, we enter in the localized not superradiant regime and also the superradiant state starts to decrease its width. Above this critical disorder strength the average width of the two subspaces became equal reaching the common value γ .

The regime for which the sensibility to disorder of the superradiant state and the subradiant states strongly differs is the *localized superradiant* regime. It is interesting to note that as we increase N , while the value of W for which Anderson transition takes place, does not change, the value of W for which the ST takes place, increases proportionally to γN . This means that the range of W where the two subspaces have different sensibility to disorder can be increased on increasing N or γ .

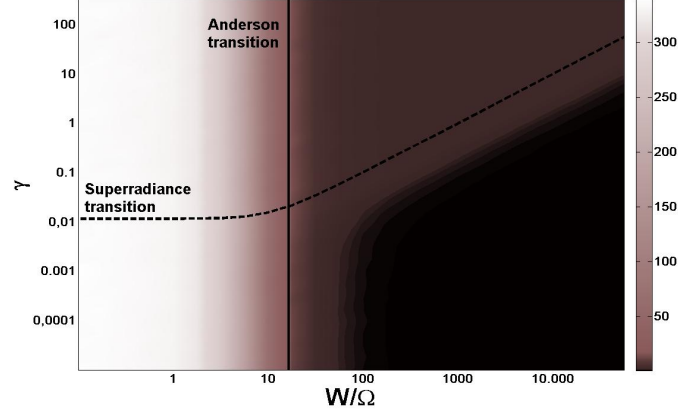
In conclusion: in the closed 3D Anderson model, the localization properties of the system are different from 1D case because all states became localized above a critical value **independent of N** . Nevertheless the sensitivity to disorder of the two subspaces of the open model is exactly the same: subradiant states are sensitive to Anderson localization, like the eigenstates of the closed system, while

the superradiant state is sensitive only to the ST.

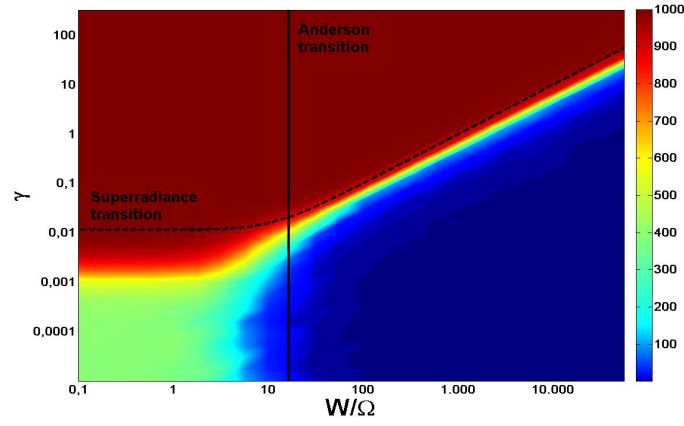
In this section we have focused our attention on the degree of localization of the eigenstates of \mathcal{H} mainly using the PR. In Figure 4.4 our results are summarized: the PR is shown as a function of both the opening γ and the disorder strength W/Ω for a fixed size of the system.

Note that we use two different colors scale for the two panels in order to increase the visibility.

Is important to note that what was known is only the behavior of the PR for the closed Anderson model, i.e. on the W/Ω axis while here we have fully analyzed the whole $(W/\Omega, \gamma)$ plane.



(a)



(b)

Figure 4.4: (a) PR of subradiant states as function of γ and W/Ω ; (b) PR of superradiant states as function of γ and W/Ω . The dashed vertical line is the Anderson transition ($W = 16.5$) and the solid line is the superradiance transition ($\gamma = D$). In both cases the system was a cube of $10 \times 10 \times 10$ sites ($N = 10^3$) and each data is obtained averaging over 5 realizations for the superradiant state while for the subradiant states an additional average over all the subradiant subspace has been done.

4.3 Structure of wave functions

For the 1D Anderson with coherent dissipation model we have found that in the limit of large disorder the structure of the averaged probability distribution (APD) is the following:

- for small opening ($\kappa \ll 1$) it consists in a sum of the APD of the closed Anderson model and a plateau proportional to $(\gamma/W)^2$, the latter being independent of N .
- for large opening ($\kappa \gg 1$) it consists in a sum of the APD of the closed Anderson model and a plateau proportional to $1/N$ and independent of γ and W .

In order to study the typical APD of the eigenstates in the 3D system we have studied the APD of the eigenstates of \mathcal{H} that are strongly peaked in the center of the cubic lattice. The APD of these states are plotted in Figure 4.5 as a function of the distance from the center of the lattice. We can see from Figure 4.5 that the APD of the eigenstates peaked in the middle of the lattice is very close to the APD of the one-dimensional model.

For small opening ($\kappa \ll 1$) we have a plateau independent of the size of the cube while for large opening ($\kappa \gg 1$) the plateau decrease as N^{-1} . Even in this case the peak of the APD has exactly the shape of the closed model (see the dashed line in Figure 4.5) and it depends from the parameters W and E in the same way.

For these reasons the framework developed for the 1D case (see subsection 3.6.1) can be very useful for this system too. In Figure 4.6 the plateau part of the APD is shown as a function of γ for different N .

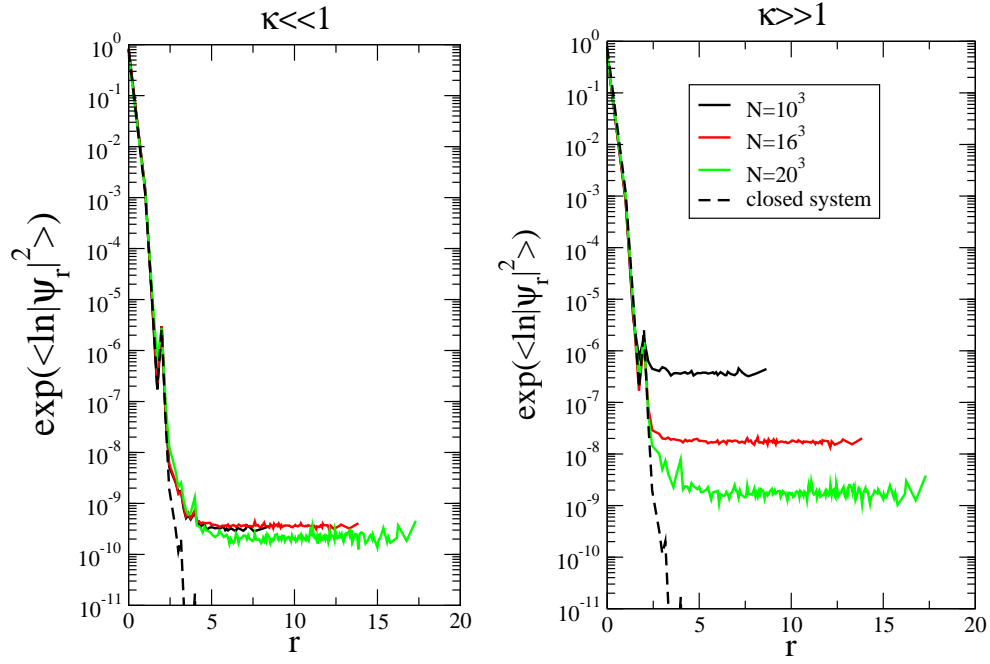


Figure 4.5: APD of all the eigenstates of \mathcal{H} that are strongly peaked in the center of the lattice as a function of the distance from the center of the lattice r . Here we fix $\gamma = 10^{-3}$ in the left panel and $\gamma = 10^2$ in the right panel. In both cases $W = 100$. Here we averaged over 10 spatial configurations. Moreover, to reduce fluctuations, we averaged the logarithm of the probability distribution.

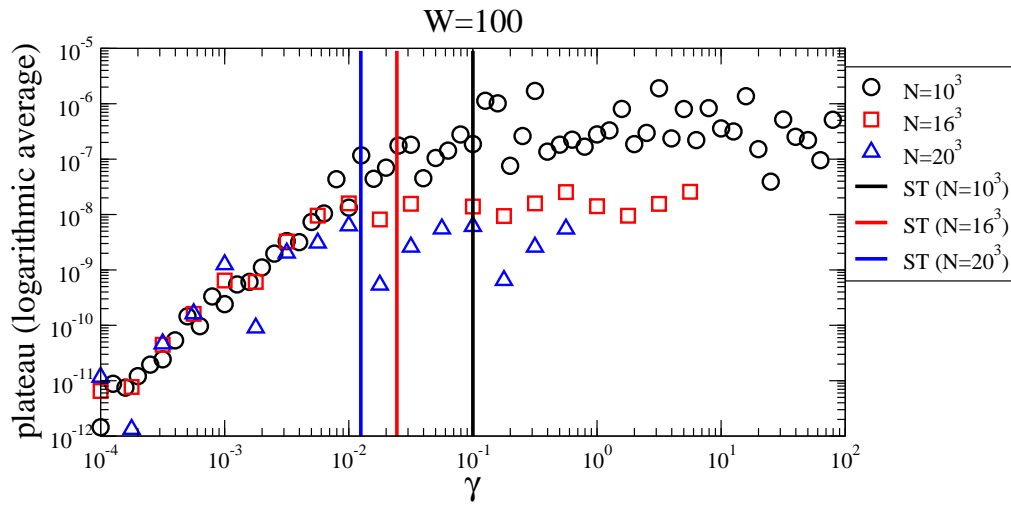


Figure 4.6: The height of the plateau as a function of γ for different N . Here $W = 100$ and each point is obtained averaging over 10 disorder realizations for $N = 10^3$ and $N = 16^3$ and 5 realizations for $N = 20^3$. The vertical solid line are the STs for different N , the colors reflect the different numerical data.

Chapter 5

Conclusions

The degree of opening and intrinsic disorder strongly affects the proprieties of mesoscopic systems in the quantum coherent regime. While in literature both opening and disorder have been extensively studied, their interplay has been not sufficiently addressed.

In this thesis we have studied their interplay in the $1D$ and $3D$ Anderson model with coherent dissipation and we have found several results, most of them not yet published. Some results about the $1D$ system have been published on the special issue of *Progress of Physics* with the title “*Quantum Physics with Non-Hermitian Operators: Theory and Experiment*”, see [28].

$1D$ Anderson model with coherent dissipation

While the disorder tends to localize the states, the opening reduces the degree of localization and in particular induces a superradiance transition, with the formation of a subradiant subspace and a superradiant state completely delocalized over all sites.

We have shown that, while for small opening all the eigenstates are similarly affected by disorder, for large opening the superradiant state and the subradiant states have a very different sensitivity to disorder. Subradiant states are sensitive to localization transition (as the eigenstates of the closed system) while the

superradiant states remains delocalized until the superradiance effect disappears.

The regime for which the behavior of the two subspaces is different is the *localized superradiant* regime, which is located between Anderson transition and the superradiance transition.

In this regime we have both superradiant and subradiant states ($\kappa > 1$), and the disorder strength is such that all the eigenstates of the closed system are exponentially localized with localization length smaller than the system size ($\xi < N$).

In the 1D Anderson model the localization threshold and the superradiance transition depends both on the sample size. Indeed if the degree of the opening (γ) is fixed the disorder strength for which $\xi < N$ behaves as

$$W_c \propto \frac{1}{\sqrt{N}} \quad (5.1)$$

and the disorder strength for which $\kappa > 1$ is proportional to N

$$W_{ST} \propto N. \quad (5.2)$$

For this reason increasing N is possible to enlarge the range of the parameters where we have the localized superradiant regime.

All these informations are well summarized in Figure 3.5 where the participation ratio (PR) is shown as a function of opening and disorder (γ and W/Ω). We remark that the behavior of the PR vs W for $\gamma = 0$ was known. Also the behavior of PR vs. γ for $W = 0$ was known. Here we have fully analyzed the whole (W, γ) plane.

We have also characterized the structure of the averaged probability distribution (APD) in the limit of large disorder:

- for small opening ($\kappa \ll 1$) it consists of two terms: the APD of the closed Anderson model and a plateau proportional to $(\gamma/W)^2$ and independent of N .
- For large opening ($\kappa \gg 1$) it consist of two terms: the APD of the closed Anderson model and a plateau proportional to $1/N$ and independent of γ and W .

The APD can be measured experimentally because it can be related to the density in the case of non-interacting particles.

3D Anderson model with coherent dissipation

In this system we have shown that the general features found in the 1D model holds also in three dimensions.

The different sensitivity to disorder of the two subspaces is confirmed and the structure of the averaged probability distribution is similar to the one-dimensional case.

Even in the 3D case, the regime for which the behavior of the two subspaces is different is the *localized superradiant* regime namely the regime for which superradiance transition is reached and all the eigenstates of the closed system are localized.

The main difference is that in 3D Anderson model the disorder strength for which Anderson transition takes place ($W \approx 16.5$) is independent of N . Nevertheless if the degree of opening is fixed the superradiance threshold depends linearly of N

$$W_{ST} \propto N. \quad (5.3)$$

This means that in 3D is possible to enlarge the range of the parameters for which the localized superradiant regime is reached increasing the size of the cubic lattice.

Applications and perspectives

The findings of our work can be used for instance to study the propagation of a photon through a cold atoms cloud: if the wavelength of the photon is larger than the system size an effective non-Hermitian long-range interaction is created. Concerning the cold atoms system, our preliminary results, confirm the general behaviors found in our *symple* model. This is not trivial because the cold atoms are not described by Anderson model. This confirms that our model is paradigmatic and can be used to understand the general features of more realistic systems.

Another important application involves the photosynthetic complexes where the transport properties are strongly affected by the interplay of superradiance and static disorder.

Our results can be applied in all those mesoscopic systems (in the quantum coherent regime) where opening and disorder are considered and for which the wavelength of the particle is larger than the typical length scale of the system.

In perspectives we plan to study also the interplay of superradiance and dynamic disorder (dephasing) instead of static disorder with direct application for quantum computation and energy transport in light harvesting systems.

Ringraziamenti

Queste pagine sono il risultato di qualche anno di passione e studio: ovviamente sarebbe stato impossibile poter portare a termine questo *viaggio* senza l'aiuto (consapevole o no) di persone, posti, viaggi, oggetti, pensieri, sogni e avvenimenti casuali.

Per questo motivo tengo a ringraziare (in ordine sparso e omettendo posti, viaggi, oggetti, pensieri, sogni e avvenimenti casuali):

la mia famiglia, senza di loro sarebbe stato tutto molto più complicato, mi ha sempre sostenuto e reso libero di fare le mie scelte, sempre. Un particolare *grazie* a mio padre: mi piace pensare che sia stato lui a insegnarmi la *passione*.

I miei amici, mille cose sono successe in questi cinque anni. Grazie per tutte le notti passate insieme, per tutte le risate e per tutte le cose che non si possono scrivere nei ringraziamenti di una tesi.

La *luna*: l'unico satellite naturale della Terra.

I miei compagni di viaggio del DMF, condividere lo stesso posto tutti i giorni, per cinque anni, ci ha reso una piccola famiglia. Le scadenze non potranno cambiare questo.

Ringrazio il Prof. Fausto Borgonovi per tutti i concetti che mi ha insegnato ma soprattutto per avermi mostrato un metodo di lavoro.

Ringrazio il Dott. Luca Celardo per tutte le ore che nell'ultimo anno mi ha dedicato e per la sua infinita disponibilità. Mi sdebiterò in un futuro.

Infine, ringrazio me stesso, per aver tenuto botta, nonostante tutto.

Bibliography

- [1] R. H. Dicke, Phys. Rev. **93**, 99 (1954).
- [2] P. W. Anderson, Phys. Rev. **109**, 1492 (1958).
- [3] G. L. Celardo and L. Kaplan, Phys. Rev. B. **79**, 155108 (2009).
- [4] A. F. Sadreev and I. Rotter, J. Phys. A-Math. Gen. **36**, 11413 (2005).
- [5] A. Ziletti, F. Borgonovi, G. L. Celardo, F. M. Izrailev, L. Kaplan and V. G. Zelevinsky, Phys Rev B **85**, 052201(2012).
- [6] G. L. Celardo, F. Borgonovi, M. Merkli, V. I. Tsifrinovich and G. P. Berman, J. Phys. Chem. C, Articles ASAP (2012)
- [7] D. J. Thouless, Phys. Rev. Lett. **61**, 2141 (1988).
- [8] F. M. Izrailev, S. Ruffo and L. Tessieri, J. Phys. A **31**, 5263 (1998).
- [9] S. Sorathia, *Scattering Properties of Open Systems of Interacting Quantum Particles*. Diss, IFUAP (2010).
- [10] P. A. Lee and T. V. Ramakrishnan, Rev. Mod. Phys. **57**, 287 (1985).
- [11] E. Akkermans, A. Gero, and R. Kaiser, Phys. Rev. Lett. **101**, 103602 (2008); R. Kaiser, J. Mod. Opt. **56**, 2082 (2009); T. Bienaime, N. Piovella, and R. Kaiser, Phys. Rev. Lett. **108**, 123602 (2012).
- [12] G. L. Celardo, F. M. Izrailev, V. G. Zelevinsky, and G. P. Berman, Phys. Lett. B **659**, 170 (2008); G. L. Celardo, F. M. Izrailev, V. G. Zelevinsky,

- and G. P. Berman, Phys. Rev. E, **76**, 031119 (2007); G. L. Celardo, S. Sorathia, F. M. Izrailev, V. G. Zelevinsky, and G. P. Berman, CP995, Nuclei and Mesoscopic Physics - WNMP 2007, ed. P. Danielewicz, P. Piecuch, and V. Zelevinsky.
- [13] F. M. Izrailev, T. Kottos and G. P. Tsironis, J. Phys. Cond. Matt. **8**, 2823 (1996).
- [14] H.-J. Stöckmann, E. Persson, Y.-H. Kim, M. Barth, U. Kuhl, and I. Rotter, Phys. Rev. E **65**, 066211 (2002); R. G. Nazmitdinov, H.-S. Sim, H. Schomerus, and I. Rotter, Phys. Rev. B **66**, 241302 (2002).
- [15] G. L. Celardo, A. M. Smith, S. Sorathia, V. G. Zelevinsky, R. A. Sen'kov, and L. Kaplan, Phys. Rev. B **82**, 165437 (2010); S. Sorathia, F. M. Izrailev, V. G. Zelevinsky, G. L. Celardo, arXiv:1107.2371v1.
- [16] F.-M. Dittes, H. L. Harney, and I. Rotter, Phys. Lett. A **153**, 451 (1991); C. Jung, M. Müller, and I. Rotter, Phys. Rev. E **60**, 114 (1999).
- [17] T. V. Shahbazyan and M. E. Raikh, Phys. Rev. B **49**, 17123 (1994).
- [18] V. V. Sokolov, I. Rotter, D. V. Savin and M. Müller, Phys. Rev. C **56**, 1031 (1997).
- [19] C. W. J. Beenakker, Rev. Mod. Phys. **69**, 731 (1997).
- [20] A. D. Zdetsis, C. M. Soukoulis, E.N. Economou and Gary S. Grest, Phys. Rev. B **32**, 7811 (1985).
- [21] J. Imry, Introduction to Mesoscopic Physics. Oxford University Press, 1997.
- [22] P. Sheng, Introduction to Wave Scattering, Localization and Mesoscopic Phenomena. Springer 2006.
- [23] S. Datta, Electronic Transport in Mesoscopic System. Cambridge University Press 1995.

- [24] N. W. Ashcroft, N. D. Mermin, Solid state Physics. Saunders College, 1976.
- [25] J. Billy, V. Josse, Z. Zuo, A. Bernard, B. Hambrecht, P. Lugan, D. Clément, L. Sanchez-Palencia, P. Bouyer and A. Aspect, Nature **453**, 891 (2008).
- [26] G. Roati, C. D’Errico, L. Fallani, M. Fattori, C. Fort, M. Zaccanti, G. Modugno, M. Modugno and M. Inguscio, Nature **453**, 895 (2008).
- [27] R. Kaiser, Journal of Modern Optics **56**, 2082 (2009).
- [28] G. L. Celardo, A. Biella, L. Kaplan, and F. Borgonovi, Fortschr. Phys., 1-11 (2012); DOI 10.1002; Special Issue on "Quantum Physics with Non-Hermitian Operators: Theory and Experiment".